COMPUTATIONAL SURVEY ON A POSTERIORI ERROR ESTIMATORS FOR NONCONFORMING FINITE ELEMENT METHODS FOR THE POISSON PROBLEM⋆

C. CARSTENSEN AND C. MERDON

ABSTRACT. This paper compares different a posteriori error estimators for nonconforming first-order Crouzeix-Raviart finite element methods for simple second-order partial differential equations. All suggested error estimators yield a guaranteed upper bound of the discrete energy error up to oscillation terms with explicit constants. Novel equilibration techniques and an improved interpolation operator for the design of conforming approximations of the discrete nonconforming finite element solution perform very well in an error estimator competition with six benchmark examples.

1. INTRODUCTION

The a posteriori error analysis of conforming FEM is well established and contained even in textbooks [BS08, Bra07, AO00, Han05, Rep08]. Although a unified framework is established [Car05], much less is known about a posteriori error analysis for nonconforming lowest-order Crouzeix-Raviart finite element methods [Ago94, HW96, DM98, Joh98, DM98, BCJ02, Ain04, Kim07, AR08, Bra09].

The Helmholtz decomposition allows a split of the error in the broken energy norm

$$\| e \|_{\mathrm{NC}}^2 \leqslant \eta^2 + \| \operatorname{Res}_{\mathrm{NC}} \|_\star^2 .$$

The first term η on the right-hand side involves contributions of the data f and is directly computable (up to quadrature errors); cf. (3.1) for an explicit representation. The second term $\| \operatorname{Res}_{\mathrm{NC}} \|_\star$ in the upper error bound is the weighted dual norm of some residual which can indeed be estimated by a posteriori error estimators for Poisson problems such as equilibration error estimators [AO00, LW04, Bra07, CM10, CDN10, Voh11], least-square error estimators [Rep08] or localisation error estimators [CF99]; another class of possible estimators exploits the identity

$$\| \operatorname{Res}_{\mathrm{NC}} \|_\star = \min_{\substack{v \in H^1(\Omega) \\ v = u_D \text{ on } \partial\Omega}} \left\| \varkappa^{1/2} (\nabla_{\mathrm{NC}} u_{\mathrm{CR}} - \nabla v) \right\|_{L^2(\Omega)}$$

of [Ain04, Car05] and Theorem 3.1.b below. Those upper bounds of $\| \operatorname{Res}_{\mathrm{NC}} \|_\star$ compute some test functions $v_{\mathrm{xyz}} \in H^1(\Omega)$ with $u = u_D$ on $\partial\Omega$ and evaluate

$$\| \operatorname{Res}_{\mathrm{NC}} \|_\star \leqslant \left\| \varkappa^{1/2} (\nabla_{\mathrm{NC}} u_{\mathrm{CR}} - \nabla v_{\mathrm{xyz}}) \right\|_{L^2(\Omega)} .$$

Three explicit designs in Subsection 4.1-4.2 provide estimators from μ_{A} after [Ain04] and μ_{AP2} after [Voh07, Ain08, Bra09], plus novel error estimators $\mu_{\mathrm{MP1RED}(0)}$ and μ_{PMRED} while

global minimisation in some discrete subspace leads in Subsection 4.3 to μ_{MP1}, μ_{MP1RED} and μ_{MP2}.

This paper concerns the Poisson model interface problem: Given a right-hand side $f \in L^2(\Omega)$, the Dirichlet data $u_D \in H^1(\Omega)$ and some bounded, piecewise constant diffusion coefficient

$$(1.1) \qquad 0 < \underline{\varkappa} \leqslant \varkappa(x) \leqslant \overline{\varkappa} < \infty \quad \text{for a.e. } x \in \Omega$$

in the domain Ω, seek $u \in H^1(\Omega)$ with

$$(1.2) \qquad -\operatorname{div}(\varkappa \nabla u) = f \text{ in } \Omega \quad \text{and} \quad u = u_D \text{ on } \partial\Omega.$$

The primal variable u will be discretised with nonconforming Crouzeix-Raviart FEMs on some regular triangulation $\mathcal{T}$ of Ω into triangles.

TABLE 1. Benchmark Poisson examples and subsection references.

Ref.	Short name	Problem data	Feature
7.1	L-shaped domain	$f \equiv 0, u_D \neq 0, \varkappa \equiv 1$	corner singularity
7.2	Slit domain	$f \equiv 1, u_D \neq 0, \varkappa \equiv 1$	slit singularity
7.3	Square domain	$f \notin P_0(\mathcal{T}), u_D \equiv 0, \varkappa \equiv 1$	oscillations
7.4	3/4-Disk domain	$f \notin P_0(\mathcal{T}), u_D \equiv 0, \varkappa \equiv 1$	osc. & corner sing.
7.5	Square domain	$f \equiv 0, u_D \neq 0, \varkappa \neq 1$	diffusion jumps
7.6	Oktagon domain	$f \equiv 0, u_D \neq 0, \varkappa \neq 1$	diffusion jumps

TABLE 2. Classes of a posteriori error estimators in this paper.

No	Classes of error estimators	Class representatives
1	interpolation	$\eta_{\mathrm{A}}, \eta_{\mathrm{MP1RED(0)}}, \eta_{\mathrm{PMRED}}, \eta_{\mathrm{AP2}}$
2	minimisation	$\eta_{\mathrm{MP1}}, \eta_{\mathrm{MP1RED(k)}}, \eta_{\mathrm{MP2}}$
3	equilibration	$\eta_{\mathrm{B}}, \eta_{\mathrm{LW}}$
4	least-square	η_{Repin}
5	localisation	η_{CF}

In this paper, the a posteriori error estimators of Table 2 compete in the 6 benchmark problems of Table 1. The 11 error estimators also give rise to adaptive mesh-refinement strategies with the overall experience that all lead to comparable mesh refinement that recovers the optimal convergence rate. Numerical evidence supports the superiority of the novel error estimator η_{PMRED} from Subsection 4.2 and η_{AP2} for adaptive a posteriori error control with efficiency indices in the range of 1.2 to 1.5. Since the overhead by η leads to only little overestimation of around 15 percent, it is indeed worth to utilise a more costly and more accurate evaluation of $\|\operatorname{Res}\|_\star$. In examples with constant coefficients, three iterations of some preconditioned conjugated gradient scheme with initial value $\mu_{\mathrm{MP1RED(0)}}$ leads to a cheap and highly efficient error estimator $\mu_{\mathrm{MP1RED(3)}}$ close to the optimum $\mu_{\mathrm{MP1RED(\infty)}}$; in examples with discontinuous coefficients the improvement after three iterations is less significant.

The remaining parts of this paper are outlined as follows. Section 2 introduces the necessary notation and preliminaries. Section 3 presents the a posteriori error analysis. Section 4 gives details on the realisations of upper bounds of $\|\operatorname{Res}_{\mathrm{NC}}\|_\star$. Section 5 deals with modifications in case of inhomogeneous boundary conditions. The novel application of equilibration techniques for a posteriori error control of nonconforming finite element methods

is introduced in Section 6. In Section 7 all estimators of Table 2 are compared with the six benchmark problems from Table 1. Section 8 draws some conclusions on the numerical experiments and adds some overall remarks.

2. Notation and Preliminaries

2.1. **Crouzeix-Raviart finite element spaces.** Given a regular triangulation $\mathcal{T}$ of the bounded Lipschitz domain $\Omega \subseteq \mathbb{R}^d$, $d = 2, 3$, into triangles with edges $\mathcal{E}$, nodes $\mathcal{N}$ and free nodes $\mathcal{M}$, the midpoints of all edges are denoted by $\mathrm{mid}(\mathcal{E}) := \{\mathrm{mid}(E) \,\big|\, E \in \mathcal{E}\}$ and the boundary edges along $\partial\Omega$ are denoted by $\mathcal{E}(\partial\Omega) := \{E \in \mathcal{E} \,\big|\, E \subseteq \partial\Omega\}$ while $\mathcal{E}(\Omega) := \mathcal{E}\backslash\mathcal{E}(\partial\Omega)$.

With the elementwise first-order polynomials $P_1(\mathcal{T})$, the nonconforming Crouzeix-Raviart finite element space reads

$$\mathrm{CR}^1(\mathcal{T}) := \{v \in P_1(\mathcal{T}) \,\big|\, v \text{ is continuous at } \mathrm{mid}(\mathcal{E})\},$$

$$\mathrm{CR}^1_0(\mathcal{T}) := \{v \in \mathrm{CR}^1(\mathcal{T}) \,\big|\, \forall E \in \mathcal{E}(\partial\Omega),\ v(\mathrm{mid}(E)) = 0\}.$$

The Crouzeix-Raviart finite element space forms a subspaces of the broken Sobolev functions $H^1(\mathcal{T}) := \{v \in L^2(\Omega) \,\big|\, \forall T \in \mathcal{T},\ v|_T \in H^1(T)\}$ with piecewise gradient $(\nabla_{\mathrm{NC}} v)|_T = \nabla v|_T$ for $v \in H^1(\mathcal{T})$ and $T \in \mathcal{T}$. The tangential component $\gamma_{\mathrm{t}}(v)$ of some vector $v \in \mathbb{R}^d$ with respect to some normal vector ν reads

$$\gamma_{\mathrm{t}}(v) := \begin{cases} v \cdot (0, -1; 1, 0)\nu & \text{if } d = 2, \\ v \times \nu & \text{if } d = 3. \end{cases}$$

2.2. **Discrete problem.** The discrete nonconforming formulation of Problem (1.2) employs $\varkappa \in P_0(\mathcal{T})$ from (1.1) and the bilinear form $a_{\mathrm{NC}} : H^1(\mathcal{T}) \times H^1(\mathcal{T}) \to \mathbb{R}$,

$$a_{\mathrm{NC}}(u, v) := \int_\Omega (\varkappa \nabla_{\mathrm{NC}} u) \cdot \nabla_{\mathrm{NC}} v \, dx := \sum_{T \in \mathcal{T}} \int_T (\varkappa \nabla u) \cdot \nabla v \, dx.$$

The (broken) energy norm $\|\!|\cdot|\!\|_{\mathrm{NC}} := a_{\mathrm{NC}}(\cdot, \cdot)^{1/2}$ is indeed positive definite on $\mathrm{CR}^1_0(\mathcal{T}) \times \mathrm{CR}^1_0(\mathcal{T})$. The right-hand side $F : L^2(\Omega) \to \mathbb{R}$ for $f \in L^2(\Omega)$ reads

$$F(v) := \int_\Omega fv \, dx \quad \text{for all } v \in L^2(\Omega).$$

The elementwise integral mean of f is denoted by

$$f_{\mathcal{T}}|_T := \fint_T f \, dx := \int_T f \, dx / |T| \quad \text{for } T \in \mathcal{T}.$$

The discrete solution $u_{\mathrm{CR}} \in \mathrm{CR}^1(\mathcal{T})$ satisfies the boundary conditions $u_{\mathrm{CR}}(\mathrm{mid}(E)) = \fint_E u_D \, ds$ for $E \in \mathcal{E}(\partial\Omega)$ and

$$a(u_{\mathrm{CR}}, v_{\mathrm{CR}}) = F(v_{\mathrm{CR}}) \quad \text{for all } v_{\mathrm{CR}} \in \mathrm{CR}^1_0(\mathcal{T}).$$

2.3. **Helmholtz decomposition.** The error $e = u - u_{\mathrm{CR}}$ is measured in the (discrete or broken) energy norm $\|\!|e|\!\|_{\mathrm{NC}} = \big\|\varkappa^{1/2} \nabla_{\mathrm{NC}} e\big\|_{L^2(\Omega)}$. To consider $d = 2, 3$ at the same time, set $k := 1$ for $d = 2$ and $k := 3$ in case of $d = 3$. One key ingredient of the error analysis is the Helmholtz decomposition of the error

$$\nabla_{\mathrm{NC}} e := \nabla u - \nabla_{\mathrm{NC}} u_{\mathrm{CR}}$$

with the $\mathrm{Curl}\, v \in L^2(\Omega; \mathbb{R}^d)$ for some $v \in H^1(\Omega; \mathbb{R}^k)$ defined by

$$\mathrm{Curl}\, v := (0, -1; 1, 0) \nabla v \text{ for } d = 2 \qquad \text{and} \qquad \mathrm{Curl}\, v := \nabla \times v \text{ for } d = 3.$$

Theorem 2.1 (Helmholtz decomposition, [GR86]). *Let Ω be a bounded (simply- or multiply-connected) Lipschitz domain. Given any $p \in L^2(\Omega; \mathbb{R}^d)$, there exist some unique $\alpha \in H_0^1(\Omega)$ and $\beta \in H^1(\Omega; \mathbb{R}^k)/\mathbb{R}$ with*

$$\varkappa p = \varkappa \nabla \alpha + \operatorname{Curl} \beta.$$

This split is orthogonal in the sense of

$$\int_{\Omega} (\varkappa p) \cdot \nabla v \, dx = \int_{\Omega} (\varkappa \nabla \alpha) \cdot \nabla v \, dx \quad \text{for all } v \in H_0^1(\Omega),$$

$$\int_{\Omega} p \cdot \operatorname{Curl} w \, dx = \int_{\Omega} (\varkappa^{-1} \operatorname{Curl} \beta) \cdot \operatorname{Curl} w \, dx \quad \text{for all } w \in H^1(\Omega; \mathbb{R}^k).$$

Proof. The Lax-Milgram lemma yields a unique solution $\alpha \in H_0^1(\Omega)$ for the first orthogonality. The remainder $q = \varkappa(p - \nabla \alpha)$ is divergence-free. Standard results in higher analysis such as Theorem 3.1 of [GR86] ensure the existence of $\beta \in H^1(\Omega; \mathbb{R}^k)$ with $q = \operatorname{Curl} \beta$. An integration by parts yields the claimed orthogonalities. □

2.4. **Adaptive mesh refinement algorithm and notation.** This section introduces our adaptive mesh-refinement algorithm.

Algorithm (ACRFEM). *INPUT coarse mesh $\mathcal{T}_0$ and $\ell := 0$.*
For level $\ell = 0, 1, 2, \dots$ until termination **do**

SOLVE discrete problem on $\mathcal{T}_\ell$ with ndof degrees of freedom.

ESTIMATE for every triangle $T \in \mathcal{T}$ with its set of edges $\mathcal{E}(T)$ and the edge patch ω_E compute

$$\eta_{\mathrm{R}}(T)^2 := |T| \, \big\| f \big\|_{L^2(T)}^2 + |T|^{1/2} \sum_{E \in \mathcal{E}(T)} \| \varkappa \|_{L^\infty(\omega_E)} \big\| [\gamma_{\mathrm{t}}(\nabla_{\mathrm{NC}} u_{\mathrm{CR}})]_E \big\|_{L^2(E)}^2.$$

MARK a minimal subset $\mathcal{M}_\ell$ of $\mathcal{T}_\ell$ such that

$$\Theta \sum_{T \in \mathcal{T}_\ell} \eta_{\mathrm{R}}(T)^2 \leqslant \sum_{T \in \mathcal{M}_\ell} \eta_{\mathrm{R}}(T)^2.$$

REFINE $\mathcal{T}_\ell$ by red-refinement of elements in $\mathcal{M}_\ell$ and red-green-blue-refinement of further elements to avoid hanging nodes and compute $\mathcal{T}_{\ell+1}$. **od**

OUTPUT Sequence of meshes $\mathcal{T}_0, \mathcal{T}_1, \dots$ with sequence of discrete solutions.

Remark 2.2. For a proof of optimality of this algorithm refer to [Rab10, MZS10].

Remark 2.3. The remaining sections are devoted to different a posteriori error estimators which motivate different refinement indicators $\eta_{\mathrm{xyz}}(T)$ specified in Sections 4-6.

3. A POSTERIORI ERROR ESTIMATION FOR POISSON PROBLEMS

This section is devoted to the a posteriori error analysis of the Poisson problem and a general reliabilty result which involves esentially two ingredients. The first one contains the right-hand side f and the elementwise oscillations of $\varkappa^{-1/2} f$,

$$\operatorname{osc}(\varkappa^{-1/2} f, \mathcal{T}) := \big\| h_{\mathcal{T}} \varkappa^{-1/2} (f - f_{\mathcal{T}}) \big\|_{L^2(\Omega)},$$

with the piecewise integral mean $f_{\mathcal{T}}$ and the piecewise constant mesh-size $h_{\mathcal{T}}$, $h_{\mathcal{T}}|_T := h_T := \text{diam}(T)$ for $T \in \mathcal{T}$. It reads

$$(3.1) \qquad \eta := \left\| \varkappa^{-1/2} f_{\mathcal{T}}/d \left(\bullet - \text{mid}(\mathcal{T}) \right) \right\|_{L^2(\Omega)} + 1/\pi \,\, \text{osc}(\varkappa^{-1/2} f, \mathcal{T}).$$

The second ingredient derives from the dual norm of the residual

$$\|\!| \text{Res}_{\text{NC}} \|\!|_\star := \sup_{\substack{v \in H^1(\Omega; \mathbb{R}^k) \\ \text{Curl}\, v \not\equiv 0}} \text{Res}_{\text{NC}}(v) / \left\| \varkappa^{-1/2} \text{Curl}\, v \right\|_{L^2(\Omega)},$$

where, for any test function $v \in H^1(\Omega; \mathbb{R}^k)$,

$$\text{Res}_{\text{NC}}(v) := \int_{\partial \Omega} v \cdot \gamma_t(\nabla u_D) \, ds - \int_\Omega \nabla_{\text{NC}} \, u_{\text{CR}} \cdot \text{Curl}\, v \, dx.$$

Theorem 3.1. *(a) Reliability of $\eta + \|\!| \text{Res}_{\text{NC}} \|\!|_\star$ holds in the sense of*

$$\|e\|_{\text{NC}}^2 = \|\!| \alpha \|\!|^2 + \|\!| \text{Res}_{\text{NC}} \|\!|_\star^2 \leqslant \eta^2 + \|\!| \text{Res}_{\text{NC}} \|\!|_\star^2$$

where $\alpha \in H_0^1(\Omega)$ stems from the Helmholtz decomposition of $\nabla e = \nabla \alpha + \varkappa^{-1} \text{Curl}\, \beta$ from Theorem 2.1.
(b) There exists an alternative characterisation of $\|\!| \text{Res}_{\text{NC}} \|\!|_\star$,

$$\|\!| \text{Res}_{\text{NC}} \|\!|_\star = \min_{\substack{v \in H^1(\Omega) \\ v = u_D \,\, on \,\, \partial\Omega}} \|u_{\text{CR}} - v\|_{\text{NC}} \leqslant \|e\|_{\text{NC}}.$$

(c) Efficiency holds in the sense of

$$\eta^2 \lesssim \|e\|_{\text{NC}}^2 + \text{osc}(\varkappa^{-1/2} f, \mathcal{T})^2.$$

Remark 3.2. For every triangle $T \in \mathcal{T}$ with set $\mathcal{E}(T)$ of edges and $s^2 := \sum_{E \in \mathcal{E}(T)} |E|^2$, it holds

$$\left\| \bullet - \text{mid}(T) \right\|_{L^2(T)}^2 = \frac{s^2 \, |T| \, d!}{(d+2)!(d+1)}.$$

This allows for a direct calculation of the leading quantity in (3.1).

Remark 3.3. The theorem is a collection of already known results extended to inhomogeneous Dirichlet conditions to cover the benchmark examples. The idea to use a Helmholtz decomposition to split up the error as in (a) dates back to [DDPV96]. The identification of the nonconforming part of the error as a residual is due to the unified approach [Car05]. The efficiency proof of the conforming part η in (c) involves bubble functions as in [Ver96, Ain04, Bra09]. A further control of $\|\!| \alpha \|\!|$ different from the overhead term η is possible with the approach in [DM98, VHS11]. It even can be rewritten as the dual norm $\|\!| \alpha \|\!| = \sup_{v \in H_0^1(\Omega)} \text{Res}(v) / \|\!| v \|\!|$ of the residual

$$\text{Res}(v) := \int_\Omega f v \, dx - \int_\Omega \varkappa \, \nabla_{\text{NC}} \, u_{\text{CR}} \cdot \nabla v \, dx \qquad \text{for } v \in H_0^1(\Omega).$$

Any known error estimator for Poisson problems can be applied to estimate the dual norm. Since in our experiments $\|\!| \text{Res} \|\!|_\star$ is smaller than $\|\!| \text{Res}_{\text{NC}} \|\!|_\star$, we here concentrate on a sharp estimation of the latter residual.

Proof. **Step 1. Helmholtz decomposition.** Consider first the Riesz representation $e^\star \in H_0^1(\Omega)$ of e with

$$\int_\Omega \nabla e^\star \cdot \nabla v \, dx = \int_\Omega \nabla_{\text{NC}} e \cdot \nabla v \, dx \qquad \text{for all } v \in H_0^1(\Omega).$$

Theorem 2.1 implies the existence of some $\alpha \in H_0^1(\Omega)$ and $\beta \in H^1(\Omega; \mathbb{R}^k)/P_0(\Omega)$ with

$$\varkappa \nabla_{\mathrm{NC}} e = \varkappa \nabla \alpha + \operatorname{Curl} \beta$$

and, with the energy norm $\|\!|\cdot|\!\| := \|\varkappa^{1/2} \nabla \cdot\|_{L^2(\Omega)}$, the error decomposition

$$\|\!|e|\!\|_{\mathrm{NC}}^2 = \int_\Omega (\varkappa \nabla \alpha) \cdot \nabla_{\mathrm{NC}} e \, dx + \int_\Omega \nabla_{\mathrm{NC}} e \cdot \operatorname{Curl} \beta \, dx = \|\!|\alpha|\!\|^2 + \|\varkappa^{-1/2} \operatorname{Curl} \beta\|_{L^2(\Omega)}^2.$$

Step 2. Proof of $\|\!|\alpha|\!\| \leqslant \eta$. Consider the nonconforming interpolation $\alpha_{\mathrm{NC}} \in \mathrm{CR}^1(\mathcal{T})$ of α defined by

$$\alpha_{\mathrm{NC}}(\operatorname{mid}(E)) := \fint_E \alpha \, ds := \int_E \alpha \, ds/|E| \quad \text{for all } E \in \mathcal{E}.$$

An integration by parts yields

(3.2) $$\int_T \nabla(\alpha - \alpha_{\mathrm{NC}}) \, dx = 0 \quad \text{for all } T \in \mathcal{T}.$$

Notice that (3.2) yields

$$\|\nabla(\alpha - \alpha_{\mathrm{NC}})\|_{L^2(T)}^2 = \int_T |\nabla \alpha|^2 \, dx - 2 \int_T \nabla \alpha \cdot \nabla \alpha_{\mathrm{NC}} \, dx + \int_T |\nabla \alpha_{\mathrm{NC}}|^2 \, dx$$
$$= \int_T |\nabla \alpha|^2 \, dx - \int_T |\nabla \alpha_{\mathrm{NC}}|^2 \, dx \leqslant \|\nabla \alpha\|_{L^2(T)}^2.$$

This allows for the estimation of the first term

$$\int_\Omega (\varkappa \nabla \alpha) \cdot \nabla_{\mathrm{NC}} e \, dx = \int_\Omega (\varkappa \nabla \alpha) \cdot \nabla u \, dx - \int_\Omega (\varkappa \nabla \alpha_{\mathrm{NC}}) \cdot \nabla_{\mathrm{NC}} u_{\mathrm{CR}} \, dx$$
$$= \int_\Omega f(\alpha - \alpha_{\mathrm{NC}}) \, dx$$
$$= \int_\Omega (f - f_{\mathcal{T}})(\alpha - \alpha_{\mathrm{NC}}) \, dx + \int_\Omega f_{\mathcal{T}}(\alpha - \alpha_{\mathrm{NC}}) \, dx.$$

An integration by parts and $(\bullet - \operatorname{mid}(T)) \cdot \nu \in P_0(\mathcal{E}(T))$ show

$$-\int_T (x - \operatorname{mid}(T)) \cdot \nabla(\alpha - \alpha_{\mathrm{NC}}) \, dx$$
$$= \int_T (\alpha - \alpha_{\mathrm{NC}}) \operatorname{div}(x - \operatorname{mid}(T)) \, dx - \int_{\partial T} (\alpha - \alpha_{\mathrm{NC}})(x - \operatorname{mid}(T)) \cdot \nu \, ds$$
$$= \int_T d(\alpha - \alpha_{\mathrm{NC}}) \, dx.$$

The orthogonality of $f - f_{\mathcal{T}}$ onto $P_0(\mathcal{T})$ allows the subtraction of the piecewise integral mean $v_{\mathcal{T}}$ of $v := \alpha - \alpha_{\mathrm{NC}}$. An elementwise Poincaré inequality with Payne-Weinberger constant $\operatorname{diam}(T)/\pi$ [PW60, Beb03] and a Cauchy inequality in $\mathbb{R}^{|\mathcal{T}|}$ yield

$$\int_\Omega (f - f_{\mathcal{T}}) v \, dx = \sum_{T \in \mathcal{T}} \int_T (f - f_{\mathcal{T}})(v - v_{\mathcal{T}}) \, dx$$
$$= \sum_{T \in \mathcal{T}} h_T/\pi \|\varkappa^{-1/2}(f - f_{\mathcal{T}})\|_{L^2(T)} \|\varkappa^{1/2} \nabla v\|_{L^2(T)}$$
$$\leqslant 1/\pi \operatorname{osc}(\varkappa^{-1/2} f, \mathcal{T}) \|\!|v|\!\|_{\mathrm{NC}}.$$

The last three estimates result in

$$\begin{aligned}
\vert\!\vert\!\vert \alpha \vert\!\vert\!\vert^2 &= \int_\Omega (\varkappa \nabla \alpha) : \nabla_{\mathrm{NC}}\, e \, dx \\
&= \int_\Omega (f - f_\mathcal{T})(\alpha - \alpha_{\mathrm{NC}})\, dx - 1/d \int_\Omega f_\mathcal{T}(x - \mathrm{mid}(T)) \cdot \nabla(\alpha - \alpha_{\mathrm{NC}})\, dx \\
&\leqslant \vert\!\vert\!\vert \alpha - \alpha_{\mathrm{NC}} \vert\!\vert\!\vert \left(1/\pi \, \mathrm{osc}(\varkappa^{-1/2} f, \mathcal{T}) + \big\Vert \varkappa^{-1/2} f_\mathcal{T}/d \, (\bullet - \mathrm{mid}(\mathcal{T})) \big\Vert_{L^2(\Omega)} \right) \\
&\leqslant \vert\!\vert\!\vert \alpha \vert\!\vert\!\vert \, \eta.
\end{aligned}$$

This leads to the assertion $\vert\!\vert\!\vert \alpha \vert\!\vert\!\vert \leqslant \eta$. $\hspace{2cm}\square$

Step 3. Proof of $\big\Vert \varkappa^{-1/2}\, \mathrm{Curl}\, \beta \big\Vert_{L^2(\Omega)} = \vert\!\vert\!\vert \mathrm{Res}_{\mathrm{NC}} \vert\!\vert\!\vert_\star$**.** The notation from Step 1, Theorem 2.1, some rotation of Curl, and an integration by parts lead, for any $v \in H^1(\Omega; \mathbb{R}^k)$, to

$$\begin{aligned}
\mathrm{Res}_{\mathrm{NC}}(v) &= \int_{\partial\Omega} v \cdot \gamma_\mathrm{t}(\nabla u_D)\, ds - \int_\Omega \nabla_{\mathrm{NC}}\, u_{\mathrm{CR}} \cdot \mathrm{Curl}\, v \, dx \\
&= \int_\Omega (\varkappa^{1/2}\, \nabla_{\mathrm{NC}}\, e) \cdot (\varkappa^{-1/2}\, \mathrm{Curl}\, v)\, dx \\
&= \int_\Omega (\varkappa^{-1/2}\, \mathrm{Curl}\, \beta) \cdot (\varkappa^{-1/2}\, \mathrm{Curl}\, v)\, dx \\
&\leqslant \big\Vert \varkappa^{-1/2}\, \mathrm{Curl}\, \beta \big\Vert_{L^2(\Omega)} \big\Vert \varkappa^{-1/2}\, \mathrm{Curl}\, v \big\Vert_{L^2(\Omega)}.
\end{aligned}$$

This implies $\vert\!\vert\!\vert \mathrm{Res}_{\mathrm{NC}} \vert\!\vert\!\vert_\star \leqslant \big\Vert \varkappa^{-1/2}\, \mathrm{Curl}_{\mathrm{NC}}\, \beta \big\Vert_{L^2(\Omega)}$. Moreover, $v = \beta$ leads to equality. $\hspace{1cm}\square$

Step 4. Proof of

$$\big\Vert \varkappa^{-1/2}\, \mathrm{Curl}\, \beta \big\Vert_{L^2(\Omega)} = \min_{\substack{v \in H^1(\Omega) \\ v = u_D \text{ on } \partial\Omega}} \big\Vert \varkappa^{1/2}(\nabla_{\mathrm{NC}}\, u_{\mathrm{CR}} - \nabla v) \big\Vert_{L^2(\Omega)}.$$

Given any $v \in H^1(\Omega)$ with $u - v = 0$ on $\partial\Omega$, Theorem 2.1 yields

$$\begin{aligned}
\big\Vert \varkappa^{-1/2}\, \mathrm{Curl}\, \beta \big\Vert_{L^2(\Omega)}^2 &= \int_\Omega \mathrm{Curl}\, \beta \cdot \nabla_{\mathrm{NC}}\, e \, dx = \int_\Omega \mathrm{Curl}\, \beta \cdot (\nabla_{\mathrm{NC}}\, u_{\mathrm{CR}} - \nabla v)\, dx \\
&\leqslant \big\Vert \varkappa^{-1/2}\, \mathrm{Curl}\, \beta \big\Vert_{L^2(\Omega)} \big\Vert \varkappa^{1/2}(\nabla_{\mathrm{NC}}\, u_{\mathrm{CR}} - \nabla v) \big\Vert_{L^2(\Omega)}.
\end{aligned}$$

Therefore

$$\big\Vert \varkappa^{-1/2}\, \mathrm{Curl}\, \beta \big\Vert_{L^2(\Omega)} \leqslant \min_{\substack{v \in H^1(\Omega) \\ v = u_D \text{ on } \partial\Omega}} \big\Vert \varkappa^{1/2}(\nabla_{\mathrm{NC}}\, u_{\mathrm{CR}} - \nabla v) \big\Vert_{L^2(\Omega)}.$$

There exists a unique minimiser in the right-hand side that equals $v := u - \alpha$ such that $\varkappa^{1/2}\, \nabla_{\mathrm{NC}}\, u_{\mathrm{CR}} - \varkappa^{1/2}\, \nabla v = -\varkappa^{-1/2}\, \mathrm{Curl}\, \beta$. In fact, this is the nature of the Helmholtz decomposition and concludes the proof. $\hspace{1cm}\square$

Step 5. Proof of $\eta^2 \lesssim \Vert e \Vert_{\mathrm{NC}}^2 + \mathrm{osc}(\varkappa^{-1/2} f, \mathcal{T})^2$**.** For a proof refer to [Bra09, Lemma 1]. $\square$

4. Realisations of upper bounds for $\vert\!\vert\!\vert \mathrm{Res}_{\mathrm{NC}} \vert\!\vert\!\vert_\star$

Seven designs for v and the estimation of $\vert\!\vert\!\vert \mathrm{Res}_{\mathrm{NC}} \vert\!\vert\!\vert_\star$ via (3.1) will be discussed in the subsequent Subsections 4.1-4.3.

4.1. **Interpolation after Ainsworth.** This subsection introduces the interpolation after Ainsworth [Ain04] that designs some piecewise linear $v_A \in H^1(\Omega)$ with respect to the original triangulation $\mathcal{T}$ by averaging on node patches $\mathcal{T}(z) := \{T \in \mathcal{T} \,|\, z \in T\}$,

$$v_A(z) := \begin{cases} u_D(z) & \text{if } z \in \mathcal{N} \backslash \mathcal{M}, \\ \left(\sum_{T \in \mathcal{T}(z)} \varkappa_T^{1/2} u_{CR}|_T(z) \right) / \left(\sum_{T \in \mathcal{T}(z)} \varkappa_T^{1/2} \right) & \text{if } z \in \mathcal{M}. \end{cases}$$

The error estimator reads

$$\eta_A^2 := \eta^2 + \left\| \varkappa^{1/2} \left(\nabla_{NC} u_{CR} - \nabla v_A \right) \right\|_{L^2(\Omega)}^2.$$

The η_A-driven ACRFEM algorithm in Subsection 2.4 replaces $\eta_R(T)^2$ by

$$\eta_A(T)^2 := \left\| \varkappa^{-1/2} f_{\mathcal{T}}/d \, (\bullet - \text{mid}(\mathcal{T})) \right\|_{L^2(T)}^2 + h_T^2/\pi^2 \left\| \varkappa^{-1/2}(f - f_{\mathcal{T}}) \right\|_{L^2(T)}^2$$
$$+ \left\| \varkappa^{1/2} \left(\nabla_{NC} u_{CR} - \nabla v_A \right) \right\|_{L^2(T)}^2.$$

For a proof of the efficiency of η_A refer to [Ain04, Theorem 6.4].

An improved interpolation from [Voh07, Ain08, Bra09] employs the auxiliary function $v^0 := u_{CR} - f_{\mathcal{T}} \psi/2 \in P_2(\mathcal{T})$ with $\psi(x) := |x - \text{mid}(T)|/2 - \fint_T |y - \text{mid}(T)| \, dy$ for $x \in T \in \mathcal{T}$. An averaging as above leads to some piecewise quadratic and continuous function $v_{AP2} \in P_2(\mathcal{T}) \cap C(\Omega)$,

$$v_{AP2}(z) := \begin{cases} u_D(z) & \text{if } z \in (\mathcal{N} \cup \text{mid}(\mathcal{E})) \cap \partial\Omega, \\ \left(\sum_{T \in \mathcal{T}(z)} \varkappa_T^{1/2} v^0|_T(z) \right) / \left(\sum_{T \in \mathcal{T}(z)} \varkappa_T^{1/2} \right) & \text{if } z \in (\mathcal{M} \cup \text{mid}(\mathcal{E})) \backslash \text{mid}(\mathcal{E}(\partial\Omega)). \end{cases}$$

The η_{AP2}-driven ACRFEM algorithm in Subsection 2.4 replaces $\eta_R(T)^2$ by

$$\eta_{AP2}(T)^2 := \left\| \varkappa^{-1/2} f_{\mathcal{T}}/d \, (\bullet - \text{mid}(\mathcal{T})) \right\|_{L^2(T)}^2 + h_T^2/\pi^2 \left\| \varkappa^{-1/2}(f - f_{\mathcal{T}}) \right\|_{L^2(T)}^2$$
$$+ \left\| \varkappa^{1/2} \left(\nabla_{NC} u_{CR} - \nabla v_{AP2} \right) \right\|_{L^2(T)}^2.$$

4.2. **Modified interpolation operator.** This subsection introduces an improved interpolation that designs some piecewise linear $v_{RED} \in H_0^1(\Omega)$ with respect to the red-refined triangulation $\text{red}(\mathcal{T})$. For simplicity, the design here restricts to $d = 2$ dimensions. A similar design for $d = 3$ dimensions is more involved. The nodes of $\text{red}(\mathcal{T})$ consists of the nodes $\mathcal{N}$ and the edge midpoints $\text{mid}(\mathcal{E})$ of $\mathcal{T}$. At the boundary the interpolation equals the nodal interpolation of u_D and on all edge midpoints it equals u_{CR},

$$v_{RED}(z) := \begin{cases} u_{CR}(z) & \text{for } z \in \text{mid}(\mathcal{E}) \backslash \text{mid}(\mathcal{E}(\partial\Omega)), \\ u_D(z) & \text{for } z \in (\mathcal{N} \cup \text{mid}(\mathcal{E})) \cap \partial\Omega, \\ v_z & \text{for } z \in \mathcal{M}. \end{cases}$$

In this way, the interpolation equals u_{CR} on all central subtriangles like T_4 in Figure 4.2 and it remains to determine the values v_z at free nodes $z \in \mathcal{M}$. They may be chosen as in the design of v_A, but we suggest to choose them locally optimal as follows. Consider the node patch $\widehat{\omega}_z$ with respect to the red-refined triangulation as in Figure 4.1. Then minimise the contribution $\left\| \varkappa^{1/2}(\nabla_{NC} u_{CR} - \nabla v) \right\|_{L^2(\widehat{\omega}_z)}$ amongst $v \in P_1(\text{red}(\mathcal{T})) \cap C(\widehat{\omega}_z)$ under the side condition of the fixed values at the edge midpoints Q_j of the adjacent edges. The value v_z at z remains the only degree of freedom in this local problem. The complete error estimator reads

$$\eta_{RED}^2 := \eta^2 + \left\| \varkappa^{1/2} \left(\nabla_{NC} u_{CR} - \nabla v_{RED} \right) \right\|_{L^2(\Omega)}^2.$$
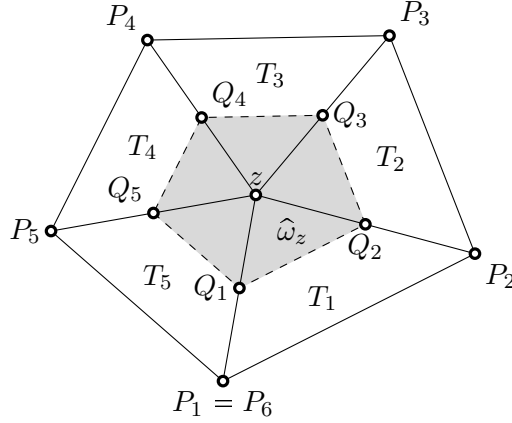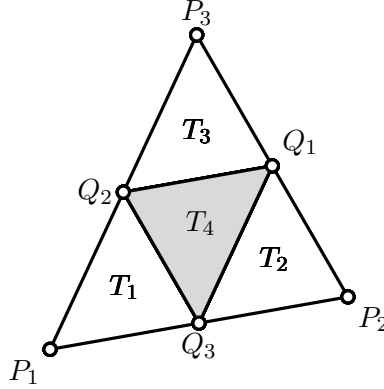
FIGURE 4.1. Interior Patch

FIGURE 4.2. Central subtriangle $T_4 = \mathrm{conv}\{\mathrm{mid}(\mathcal{E}(T))\}$ in $\mathrm{red}(T)$ for $T \in \mathcal{T}$.

The η_{RED}-driven ACRFEM algorithm in Subsection 2.4 replaces $\eta_{\mathrm{R}}(T)^2$ by

$$\eta_{\mathrm{RED}}(T)^2 := \left\| \varkappa^{-1/2} f_{\mathcal{T}}/d \; (\bullet - \mathrm{mid}(\mathcal{T})) \right\|_{L^2(T)}^2 + h_T^2/\pi^2 \left\| \varkappa^{-1/2}(f - f_{\mathcal{T}}) \right\|_{L^2(T)}^2$$
$$+ \left\| \varkappa^{1/2} \left(\nabla_{\mathrm{NC}} \, u_{\mathrm{CR}} - \nabla \, v_{\mathrm{RED}} \right) \right\|_{L^2(T)}^2.$$

We distinguish between the optimal version η_{PMRED}, where v_z is chosen patchwise minimal (PM) as described above, and $\eta_{\mathrm{MP1RED}(0)}$ with the suboptimal choice v_z as in Subsection 4.1. This can be seen as a modification $v_{\mathrm{MP1RED}(0)}$ of v_{A} at the edge midpoints.

4.3. **Optimal choices.** The optimal $v \in P_1(\mathcal{T}) \cap C(\Omega)$ is attained at the solution u_C of the conforming formulation of the Poisson problem, since the nodal basis functions are included in $CR^1(\mathcal{T})$ and hence

$$\int_\Omega f v_C \, dx = \int_\Omega (\varkappa \nabla_{\mathrm{NC}} \, u_{\mathrm{CR}}) \cdot \nabla \, v_C \, dx$$
$$= \int_\Omega (\varkappa \nabla \, u_C) \cdot \nabla \, v_C \, dx \quad \text{for all } v_C \in P_1(\mathcal{T}) \cap H_0^1(\Omega).$$

For comparison, we also compute the optimal $v_{\mathrm{MP1RED}} \in P_1(\mathrm{red}(\mathcal{T})) \cap C(\Omega)$ on the red-refined triangulation $\mathrm{red}(\mathcal{T})$ and the optimal piecewise quadratic $v_{\mathrm{MP2}} \in P_2(\mathcal{T}) \cap C(\Omega)$. Note that they do not have to equal the corresponding conforming solutions. To reduce

the computational costs of v_{MP1RED} one might use $v_{\text{MP1RED}(0)}$ as an initial guess for some iterative solver to draw near the optimal value. We use a preconditioned conjugate gradients algorithm and stop at the third iterate $v_{\text{MP1RED}(3)}$. For the preconditioner we use the diagonal of the system matrix also known as Jacobi preconditioner. The associated error estimators $\eta_{\text{MP1RED}(0)}$, η_{MP1}, η_{MP2}, η_{MP1RED} and $\eta_{\text{MP1RED}(3)}$ and adaptive algorithms based on local refinement indicators $\eta_{\text{xyz}}(T)^2$ are defined in the same manner as for η_A.

5. Inhomogeneous boundary conditions

The designs of the test function v of Section 4 illustrate that inhomogeneous boundary data u_D may not be resolved exactly. Hence, let $v = v_D$ on $\partial\Omega$ and extend the boundary values $w_D = u_D - v_D$ on $\partial\Omega$ to some function $w_D \in H^1(\Omega)$ after [BCD04]. Since w_D satisfies $u - (v + w_D) \in H_0^1(\Omega)$,

$$\| \operatorname{Res}_{\text{NC}} \|_\star = \min_{\substack{\widehat{v} \in H^1(\Omega) \\ \widehat{v} = u_D \text{ on } \partial\Omega}} \| u_{\text{CR}} - \widehat{v} \|_{\text{NC}} \leqslant \| u_{\text{CR}} - (v + w_D) \|_{\text{NC}} \leqslant \| u_{\text{CR}} - v \|_{\text{NC}} + \| w_D \|.$$

The term $\| w_D \|$ can be computed and may be of higher order for a reasonable choice of v_D.

Theorem 5.1. *Assume that $u_D \in H^1(\partial\Omega) \cap C(\partial\Omega)$ satisfies $u_D \in H^2(E)$ for all $E \in \mathcal{E}(\partial\Omega)$ and set $v_D = \mathcal{I} u_D := \sum_{z \in \mathcal{N} \setminus \mathcal{M}} u_D(z) \varphi_z$. Let $\partial_{\mathcal{E}}^2 u_D / \partial s^2$ denote the edgewise second surface derivative of u_D along $\partial\Omega$. Then there exists $w_D \in H^1(\Omega)$ and some constant*

$$C_1 := \max_{E \in \mathcal{E}(\partial\Omega)} \left(\frac{\pi\delta + h_E}{\pi^2 \sqrt{2 h_E \varrho}} \right) \lesssim 1$$

(where $\delta := \max_{x \in E} |x - \operatorname{mid}(T_E)|$ and $\varrho := \operatorname{dist}(E, \operatorname{mid}(T_E))$ of the adjacent triangle T_E of $E \in \mathcal{E}(\partial\Omega)$ depend only on interior angles in $\mathcal{T}$) with

$$w_D|_{\partial\Omega} = u_D - v_D \quad and \quad \| w_D \| \leqslant C_1 \big\| h_{\mathcal{E}}^{3/2} \varkappa^{1/2} \partial_{\mathcal{E}}^2 u_D / \partial s^2 \big\|_{L^2(\partial\Omega)}.$$

Proof. The proof employs an explicit construction of w_D from [BCD04] and is repeated here to calculate C_1 for guaranteed error control for $d = 2$. The case $d = 3$ allows similar arguments. Consider a triangle $T_E = \operatorname{conv}\{P_1, P_2, P_3\} \in \mathcal{T}$ with a Dirichlet edge $E := \operatorname{conv}\{P_2, P_3\} \in \mathcal{E}(\partial\Omega)$. The connection between the center of gravity $\operatorname{mid}(T_E)$ and the three vertices of T_E results in three subtriangles of the same area depicted in Figure 5.1. Let K_E denote the subtriangle of Figure 5.1 with $E = \partial K_E \cap \partial T_E$. For every point $x \in K_E \setminus \{\operatorname{mid}(T_E)\}$ there exist some unique $\zeta_x \in E$ and $0 < \lambda_x \leqslant 1$, with $x = (1 - \lambda_x) \operatorname{mid}(T_E) + \lambda_x \zeta_x$. Then,

$$w_D(x)|_{K_E} = \begin{cases} \lambda_x (u_D(\zeta_x) - v_D(\zeta_x)) & \text{for } x \in K_E \setminus \{\operatorname{mid}(T_E)\}, \\ 0 & \text{else.} \end{cases}$$

On all other triangles w_D is set to zero.

Without loss of generality, we assume $\operatorname{mid}(T_E) = 0 \in \mathbb{R}^2$. Polar coordinates yield the parameterisation

$$K_E = \{ x = (r\cos(\varphi), r\sin(\varphi)) \,|\, \alpha < \varphi < \beta, \ 0 < r < R(\varphi) := |\zeta_x| \}$$

where α and β are the angles at the points P_2 and P_3, respectively. For $x \in K_E$ and $\zeta_x = \varrho \nu_E + s \tau_E$ with normal vector ν_E, tangential vector τ_E and height $\varrho = \operatorname{dist}(\operatorname{mid}(T_E), E)$, it holds $R(\varphi)^2 = |\zeta_x|^2 = \varrho^2 + s^2$. Furthermore, for $g(\varphi) := u_D(\zeta_x) - v_D(\zeta_x)$, it holds $w_D(x) = r/R(\varphi) g(\varphi)$ and

$$|\nabla w_D(r, \varphi)|^2 = |\partial w_D / \partial r|^2 + |\partial w_D / \partial\varphi|^2 / r^2$$

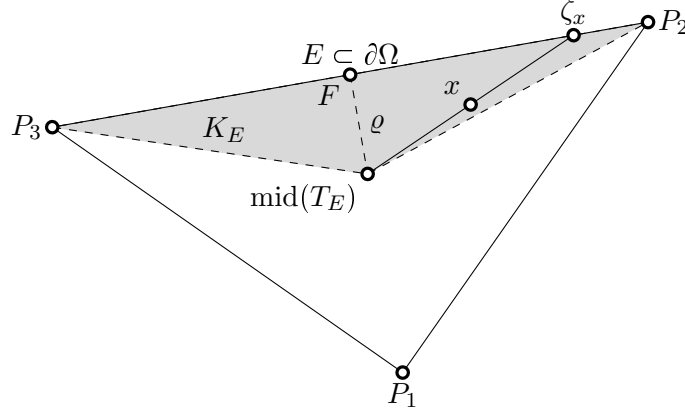$$= |g(\varphi)/R(\varphi)|^2 + \big| R(\varphi) g'(\varphi) - R' g(\varphi) \big|^2 / R^2(\varphi).$$

FIGURE 5.1. Visualisation of notation for the construction of w_D in the proof of Theorem 5.1.

The expressions

$$R(\varphi) = \varrho/\cos(\varphi - \chi) \quad \text{and} \quad s(\varphi) = \varrho \tan(\varphi - \chi),$$

where χ is the angle of theperpendicular point F, depicted in Figure 5.1, yield the differentials

$$R'(\varphi) = s(\varphi)R(\varphi)/\varrho, \qquad s'(\varphi) = \varrho/\cos^2(\varphi - \chi),$$

$$g'(\varphi) = \frac{\partial g}{\partial s}\frac{\partial s}{\partial \varphi} = \frac{\partial g}{\partial s}R(\varphi)^2/\varrho.$$

Hence,

$$\int_{K_E} |\nabla w_D(x)|^2 \, dx = \int_\alpha^\beta \int_0^{R(\varphi)} |\nabla w_D(r, \varphi)|^2 \, r \, dr \, d\varphi = \frac{1}{2} \int_\alpha^\beta g^2 + \left(R^2 g'/\varrho - gs/\varrho\right)^2 \, d\varphi.$$

The transformation $d\varphi = \cos^2(\varphi - \chi) \, ds/\varrho = \varrho \, ds/(\varrho^2 + s^2)$ yields

$$\int_\alpha^\beta g(\varphi)^2 \, d\varphi = \int_a^b g(s)^2 \varrho/(\varrho^2 + s^2) \, ds \leqslant 1/\varrho \left\|g\right\|_{L^2(E)}.$$

The same transformation and the Young inequality for some $\lambda > 0$ in the second summand show

$$\int_\alpha^\beta \left(R^2 g'/\varrho - gs/\varrho\right)^2 \, d\varphi = \int_a^b \left(\frac{R^2}{\varrho}\frac{\partial g}{\partial s} - gs/\varrho\right)^2 \varrho/(\varrho^2 + s^2) \, ds$$

$$\leqslant \int_a^b (1 + \lambda)\frac{R^2}{\varrho}\left(\frac{\partial g}{\partial s}\right)^2 + (1 + 1/\lambda)\frac{s^2}{\varrho(\varrho^2 + s^2)}g^2 \, ds.$$

The estimate $s^2/(\varrho(\varrho^2 + s^2)) \leqslant 1/\varrho$ results in

$$\int_\alpha^\beta \left(R^2 g'/\varrho - gs/\varrho\right)^2 \, d\varphi \leqslant (1 + \lambda)\max_\varphi R(\varphi)^2/\varrho \left\|\partial g/\partial s\right\|_{L^2(E)}^2 + (1 + 1/\lambda)/\varrho \left\|g\right\|_{L^2(E)}^2.$$

For $v_D := \mathcal{I}u_D$ the Friedrichs inequality for $g \in H_0^1(E)$ and the Poincaré inequality for $\partial g/\partial s$ yield

$$
\int_{K_E} |\nabla\, w_D(x)|^2 \, dx \leqslant \frac{(1+\lambda)\max_\varphi R(\varphi)^2}{2\varrho} \big\|\partial g/\partial s\big\|_{L^2(E)}^2 + \frac{2+1/\lambda}{2\varrho}\big\|g\big\|_{L^2(E)}^2
$$

$$
\leqslant \left(\frac{(1+\lambda)\delta^2}{2h_E\pi^2\varrho} + \frac{(2+1/\lambda)h_E}{2\pi^4\varrho}\right)\big\|h_E^{3/2}\partial^2 g/\partial s^2\big\|_{L^2(E)}^2.
$$

Elementary calculations lead to the optimal $\lambda = h_E/(\pi\delta)$ and the claimed constant C_1. Since $\varkappa \in P_0(\mathcal{T})$ is constant on $K_E \subset T$ it acts as an global constant that can be easily multiplied to both sides. This concludes the proof. $\qquad\square$

Remark 5.2. For right isosceles triangles and optimal λ numerical calculations suggest the constant $C_1 = .6388$. If $v|_{\partial\Omega}$ is the nodal interpolation of u_D on the red-refined triangulation, w_D can be designed on the red-refined triangulation with halfed edge lengths and the constant reduces to $C_1 = .6388/2^{3/2} = .2258$.

Remark 5.3. Due to the inhomogeneous boundary conditions all error estimators η_{xyz}^2 in Section 4 have to be replaced by

$$
\eta^2 + \left(\big\|\varkappa^{1/2}\,(\nabla_{\text{NC}}\,u_{\text{CR}} - \nabla\,v_{\text{xyz}})\,\big\|_{L^2(\Omega)} + C_1\big\|h_{\mathcal{E}}^{3/2}\varkappa^{1/2}\partial_{\mathcal{E}}^2 u_D/\partial s^2\big\|_{L^2(\partial\Omega)}\right)^2.
$$

The refinement indicators $\eta_{\text{xyz}}(T)^2$ are accordingly replaced by

$$
\eta_{\text{xyz}}(T)^2 + C_1^2\big\|h_{\mathcal{E}}^{3/2}\varkappa^{1/2}\partial_{\mathcal{E}}^2 u_D/\partial s^2\big\|_{L^2(\partial T\cap\partial\Omega)}^2.
$$

6. EQUILIBRATION ESTIMATORS

This section concerns the application of equilibration techniques known from Poisson problems to compute upper bounds for $\|\!|\operatorname{Res}_{\text{NC}}\|\!|_\star$. At this point we only discuss the case $d = 2$ and $k = 1$ as the modifications to $d = 3$ are more involved.

6.1. **Introduction of equilibration.** Given some $q \in H(\operatorname{div}, \Omega)$, an integration by parts leads, for any $v \in H^1(\Omega)$, to

$$
\operatorname{Res}_{\text{NC}}(v) = \int_{\partial\Omega} v\;\gamma_{\text{t}}(\nabla u_D)\,ds - \int_\Omega \operatorname{Curl}_{\text{NC}} u_{\text{CR}} \cdot \nabla\,v\,dx
$$

$$
(6.1)\qquad = \int_\Omega \operatorname{div} q\,v\,dx + \int_{\partial\Omega} v(\gamma_{\text{t}}(\nabla u_D) - q\cdot\nu)\,ds + \int_\Omega (q - \operatorname{Curl}_{\text{NC}} u_{\text{CR}}) \cdot \nabla\,v\,dx.
$$

A careful but straightforward estimation of (6.1) proves the following a posteriori error control. The Friedrichs constant is given as

$$
C_F := \sup\left\{\big\|f\big\|_{L^2(\Omega)}\;:\;f \in H_0^1(\Omega)\;\&\;\big\|\nabla f\big\|_{L^2(\Omega)} = 1\right\}.
$$

Theorem 6.1. *Given* $q \in H(\operatorname{div}, \Omega)$ *with*

$$
(6.2)\qquad\qquad \int_E (\gamma_{\text{t}}(\nabla u_D) - q\cdot\nu)\,ds = 0 \quad \text{for all } E \in \mathcal{E}(\partial\Omega)
$$

and $C_2 := \sqrt{2/(d\pi) + 1/\pi^2}\,\max_{E\in\mathcal{E}(\partial\Omega)}\operatorname{diam}(\omega_E)/|\omega_E|^{1/2}$, *it holds*

$$
\|\!|\operatorname{Res}_{\text{NC}}\|\!|_\star \leqslant C_F\big\|\varkappa^{1/2}\operatorname{div} q\big\|_{L^2(\Omega)} + \big\|\varkappa^{1/2}(q - \operatorname{Curl}_{\text{NC}} u_{\text{CR}})\big\|_{L^2(\Omega)}
$$

$$
+ C_2\big\|(h_{\mathcal{E}}\varkappa)^{1/2}(\gamma_{\text{t}}(\nabla u_D) - q\cdot\nu)\big\|_{L^2(\partial\Omega)}.
$$

Proof. Set $g := \gamma_{\mathrm{t}}(\nabla u_D) - q \cdot \nu$ and select one adjacent triangle $\overline{\omega_E} := \mathrm{conv}\{\{P\} \cup E\}$ for every boundary edge $E \in \mathcal{E}(\partial\Omega)$. Given $v \in H^1(\Omega)$, fix $v_E := \fint_{\omega_E} v \, dx$. The trace identity (from an integration by parts and $\mathrm{div}(x) = d$) reads

$$\left\| v - v_E \right\|_{L^2(E)}^2 = \int_E (v - v_E)^2 \, ds$$
$$= \frac{|E|}{|\omega_E|} \int_{\omega_E} (v - v_E)^2 \, dx + \frac{|E|}{d \, |\omega_E|} \int_{\omega_E} (x - P) \cdot \nabla((v - v_E)^2) \, dx.$$

It holds

$$\int_{\omega_E} (x - P) \cdot \nabla((v - v_E)^2) \, dx \leqslant 2 \, \mathrm{diam}(\omega_E) \int_{\omega_E} (v - v_E) \, \nabla(v - v_E) \, dx$$
$$\leqslant 2 \, \mathrm{diam}(\omega_E) \left\| v - v_E \right\|_{L^2(\omega_E)} \left\| \nabla v \right\|_{L^2(\omega_E)}.$$

Together with a Poincaré inequality this yields

$$\left\| v - v_E \right\|_{L^2(E)}^2 \leqslant \mathrm{diam}(\omega_E)^2 \, |E| \, / \, |\omega_E| \, \left(2/(d\pi) + 1/\pi^2 \right) \left\| \nabla v \right\|_{L^2(\omega_E)}^2 \leqslant C_2^2 \, |E| \, \left\| \nabla v \right\|_{L^2(\omega_E)}^2.$$

We use $\int_E g \, ds = 0$ for $E \in \mathcal{E}(\partial\Omega)$ to estimate the second term in (6.1) by

$$\int_{\partial\Omega} v(\gamma_{\mathrm{t}}(\nabla u_D) - q \cdot \nu) \, ds = \sum_{E \in \mathcal{E}(\partial\Omega)} \int_E g(v - v_E) \, ds$$
$$\leqslant \sum_{E \in \mathcal{E}(\partial\Omega)} \left\| \varkappa^{1/2} g \right\|_{L^2(E)} \left\| \varkappa^{-1/2}(v - v_E) \right\|_{L^2(E)}$$
$$\leqslant C_2 \left\| (h_{\mathcal{E}} \varkappa)^{1/2} (\gamma_{\mathrm{t}}(\nabla u_D) - q \cdot \nu) \right\|_{L^2(\partial\Omega)} \left\| \varkappa^{-1/2} \nabla v \right\|_{L^2(\Omega)}.$$

The Friedrichs inequality in the first term of (6.1) gives

$$\int_\Omega \mathrm{div} \, q \, v \, dx \leqslant C_F \left\| \varkappa^{1/2} \, \mathrm{div} \, q \right\|_{L^2(\Omega)} \left\| \varkappa^{-1/2} \nabla v \right\|_{L^2(\Omega)}.$$

The last two estimates plus a Poincaré inequality in the second term of (6.1) conclude the proof. $\qquad\square$

Equilibration estimators techniques for Poisson problems [AO00, LW04, Bra07, CM10, CDN10, Voh11], least-square methods [Rep08] or mixed methods [GR86, Bra07] compute $q \in H(\mathrm{div}, \Omega)$ where

$$q \cdot \nu \approx \gamma_{\mathrm{t}}(\nabla u_D) \quad \text{along } \partial\Omega$$

acts as Neumann boundary conditions on q. The particular choice $q \cdot \nu_E|_E := \fint_E \gamma_{\mathrm{t}}(\nabla u_D) \, ds$ for $E \in \mathcal{E}(\partial\Omega)$ leads to boundary oscillations of $\varkappa^{1/2} \, \gamma_{\mathrm{t}}(\nabla u_D)$,

$$\mathrm{osc}(\varkappa^{1/2} \, \gamma_{\mathrm{t}}(\nabla u_D), \mathcal{E}(\partial\Omega)) := \left\| (h_{\mathcal{E}} \varkappa)^{1/2} (\gamma_{\mathrm{t}}(\nabla u_D) - q \cdot \nu_E) \right\|_{L^2(\partial\Omega)},$$

Three possible designs are given in Subsections 6.2-6.5.

Remark 6.2. For triangulations that consist only of rectangular triangles, it holds $C_2 \leqslant 2\sqrt{1/\pi + 1/\pi^2} = 1.2956$. This constant is used for all numerical computations of Section 7.

Remark 6.3. To guarantee the solvability of local problems for certain a posteriori error estimators one has to check that the nodal basis functions φ_z for all $z \in \mathcal{N}$ (also the nodes at

the boundary to impose Neumann conditions on q at the Dirichlet boundary) are included in the kernel of $\mathrm{Res_{NC}}$. In fact, an elementwise integration by parts shows

$$\mathrm{Res_{NC}}(\varphi_z) = \int_{\partial\Omega} \varphi_z \cdot \gamma_\mathrm{t}(\nabla u_D)\, ds - \int_\Omega \nabla u_\mathrm{CR} \cdot \mathrm{Curl}\, \varphi_z\, dx$$

$$= \sum_{T\in\mathcal{T}} \int_{\partial\Omega\cap\partial T} u_D\,\mathrm{Curl}\, \varphi_z \cdot \nu\, ds - \int_{\partial T} u_\mathrm{CR}\,\mathrm{Curl}\, \varphi_z \cdot \nu_T\, ds$$

$$= \sum_{T\in\mathcal{T}} \sum_{E\in\mathcal{E}(T)} \left(\fint_{\partial\Omega\cap E} u_D\, ds - u_\mathrm{CR}(\mathrm{mid}(E)) \right) \int_E \mathrm{Curl}\, \varphi_z \cdot \nu_T\, ds.$$

All contributions on inner edges are zero, because u_CR is continuous in edge midpoints, $\mathrm{Curl}\,\varphi_z \cdot \nu = 0$ along $\partial\omega_z$, and $\mathrm{Curl}\,\varphi_z$ has no normal jumps. Since

$$u_\mathrm{CR}(\mathrm{mid}(E)) = \fint_E u_D\, ds \quad \text{for all } E\in\mathcal{E}(\partial\Omega),$$

the contributions on boundary edges $\mathcal{E}(\partial\Omega)$ vanish. Hence $\mathrm{Res_{NC}}(\varphi_z) = 0$.

6.2. **Equilibration after Luce and Wohlmuth.** The technique by Luce and Wohlmuth [LW04] employs the dual triangulation $\mathcal{T}^\star$ which connects each $\mathrm{mid}(T)$ with adjacent nodes and edge midpoints and so devides every $T\in\mathcal{T}$ into $(d+1)!$ triangles of area $|T|/6$.

Consider some node $z\in\mathcal{N}(\mathcal{T})$ and its nodal basis function $\varphi_z^\star$ with the fine patch $\omega_z^\star := \{\varphi_z^\star > 0\}$ of the dual triangulation $\mathcal{T}^\star$ and its neighbouring triangles $\mathcal{T}^\star(z) := \{T^\star \in \mathcal{T}^\star \mid z\in \mathcal{N}^\star(T^\star)\}$ and adjacent edges $\mathcal{E}^\star(z) = \{E\in\mathcal{E}^\star \mid z\in E\}$. Since $\mathrm{Curl_{NC}}\, u_\mathrm{CR} \in P_0(\mathcal{T};\mathbb{R}^d)$ is continuous along $\partial\omega_z^\star \cap T$ for any $T\in\mathcal{T}$, $q\cdot\nu = \mathrm{Curl_{NC}}\, u_\mathrm{CR}\cdot\nu \in P_0(\mathcal{E}^\star(\partial\omega_z^\star))$ is well-defined on the boundary edges $\mathcal{E}^\star(\partial\omega_z^\star)$ of $\omega_z^\star$. The original Luce-Wohlmuth design does not involve Neumann boundary conditions, but they may be easily included by some interpolation $g^\star \in P_0(\mathcal{E}^\star(\partial\Omega))$ of $\gamma_\mathrm{t}(\nabla u_D)$ defined by

$$g^\star|_E := 2\int_E \varphi_z\, \gamma_\mathrm{t}(\nabla u_D)\, ds\,/\,|E| \quad \text{for } z\in\mathcal{N}(\partial\Omega), E\in\mathcal{E}^*(\partial\omega_z)\cap\mathcal{E}^\star(z).$$

This leads to the bound

$$\int_{\partial\Omega} (\gamma_\mathrm{t}(\nabla u_D) - g^\star)\, v\, ds \leqslant C_2 \big\|(h_\mathcal{E}\varkappa)^{1/2}(\gamma_\mathrm{t}(\nabla u_D) - g^\star)\big\|_{L^2(\partial\Omega)} \|\!|v|\!\|$$

with the calculated constant C_2 from Remark 6.2. The modified Luce-Wohlmuth estimator similar to [Voh11] computes the minimiser

$$q_\mathrm{LW}|_{\omega_z^\star} := \underset{\tau_h\in Q(\mathcal{T}^\star(z))}{\mathrm{argmin}} \big\|\varkappa^{1/2}(g - \tau_h)\big\|_{L^2(\omega_z^\star)}$$

in the set

$$Q(\mathcal{T}^\star(z)) := \big\{\tau_h \in RT_0(\mathcal{T}^\star(z)) \mid \mathrm{div}\,\tau_h = 0 \text{ in } \omega_z^\star \,\&\, \tau_h\cdot\nu = \mathrm{Curl_{NC}}\, u_\mathrm{CR}\cdot\nu \text{ along } \partial\omega_z^\star\backslash\partial\Omega$$

$$\&\, \tau_h\cdot\nu = g^\star \text{ along } \partial\omega_z^\star \cap \partial\Omega\big\}.$$

The Luce-Wohlmuth error estimator reads

$$\eta_\mathrm{LW}^2 := \eta^2 + \left(\big\|\varkappa^{1/2}(q_\mathrm{LW} - \mathrm{Curl_{NC}}\, u_\mathrm{CR})\big\|_{L^2(\Omega)} + C_2\big\|(h_\mathcal{E}\varkappa)^{1/2}(\gamma_\mathrm{t}(\nabla u_D) - q_\mathrm{LW}\cdot\nu)\big\|_{L^2(\partial\Omega)} \right)^2.$$

The η_LW-driven ACRFEM algorithm in Subsection 2.4 replaces $\eta_\mathrm{R}(T)^2$ by

$$\eta_\mathrm{LW}(T)^2 := \big\|\varkappa^{-1/2} f_\mathcal{T}/d\,(\bullet - \mathrm{mid}(\mathcal{T}))\big\|_{L^2(T)}^2 + h_T^2/\pi^2 \big\|\varkappa^{-1/2}(f - f_\mathcal{T})\big\|_{L^2(T)}^2$$

$$+ \big\|\varkappa^{1/2}(q_\mathrm{LW} - \mathrm{Curl_{NC}}\, u_\mathrm{CR})\big\|_{L^2(T)}^2 + C_2^2\big\|(h_\mathcal{E}\varkappa)^{1/2}(\gamma_\mathrm{t}(\nabla u_D) - q_\mathrm{LW}\cdot\nu)\big\|_{L^2(\partial T\cap\partial\Omega)}^2.$$

6.3. **Equilibration after Braess.** Braess [Bra07] designs patchwise broken Raviart-Thomas functions $r_z \in RT_{-1}(\mathcal{T}(z)) := \{q \in L^2(\omega_z) \,|\, q|_T \in RT_0(T) \text{ for any } T \in \mathcal{T}(z)\}$ that satisfy $\operatorname{div} q_z \equiv 0$,

$$
\begin{aligned}
[r_z \cdot \nu_E]_E &= -[\operatorname{Curl}_{\mathrm{NC}} u_{\mathrm{CR}} \cdot \nu_E]_E/2 && \text{on } E \in \mathcal{E}(z) \cap \mathcal{E}(\partial\Omega), \\
r_z \cdot \nu &= 0 && \text{along } \partial\omega_z \backslash \mathcal{E}(\partial\Omega), \\
r_z \cdot \nu &= \int_E \varphi_z \, \gamma_{\mathrm{t}}(\nabla u_D) \, ds && \text{along } \partial\omega_z \cap \mathcal{E}(\partial\Omega).
\end{aligned}
$$

The solution r_z of these problems is unique up to multiplicatives of $\operatorname{Curl} \varphi_z$ and may be chosen such that $\left\| \varkappa^{1/2} r_z \right\|_{L^2(\omega_z)}$ is minimal. Eventually, the quantity $q_{\mathrm{B}} := \operatorname{Curl}_{\mathrm{NC}} u_{\mathrm{CR}} + \sum_{z \in \mathcal{N}} r_z \in RT_0(\mathcal{T})$ satisfies

$$
\left\| \gamma_{\mathrm{t}}(\nabla u_D) - q_{\mathrm{B}} \cdot \nu \right\|_{L^2(\partial\Omega)} \leqslant C_2 \operatorname{osc}(\varkappa^{1/2} \gamma_{\mathrm{t}}(\nabla u_D), \mathcal{E}(\partial\Omega)).
$$

The estimator reads

$$
\eta_{\mathrm{B}}^2 := \eta^2 + \left(\left\| \varkappa^{1/2}(q_{\mathrm{B}} - \operatorname{Curl}_{\mathrm{NC}} u_{\mathrm{CR}}) \right\|_{L^2(\Omega)} + C_2 \operatorname{osc}(\varkappa^{1/2} \gamma_{\mathrm{t}}(\nabla u_D), \mathcal{E}(\partial\Omega)) \right)^2.
$$

The η_{B}-driven ACRFEM algorithm in Subsection 2.4 replaces $\eta_{\mathrm{R}}(T)^2$ by

$$
\begin{aligned}
\eta_{\mathrm{B}}(T)^2 := \, & \left\| \varkappa^{-1/2} f_{\mathcal{T}}/d \, (\bullet - \operatorname{mid}(\mathcal{T})) \right\|_{L^2(T)}^2 + h_T^2/\pi^2 \left\| \varkappa^{-1/2}(f - f_{\mathcal{T}}) \right\|_{L^2(T)}^2 \\
& + \left\| \varkappa^{1/2}(q_{\mathrm{B}} - \operatorname{Curl}_{\mathrm{NC}} u_{\mathrm{CR}}) \right\|_{L^2(T)}^2 + C_2^2 \operatorname{osc}(\varkappa^{1/2} \gamma_{\mathrm{t}}(\nabla u_D), \mathcal{E}(T) \cap \mathcal{E}(\partial\Omega))^2.
\end{aligned}
$$

6.4. **Least-square estimator after Repin.** Following Repin [Rep08], we seek the best $q_{\mathrm{Repin}} \in RT_0(\mathcal{T})$ with (6.2) and a priori unconstrained divergence via a series of least square problems that minimises

$$
\min_{\substack{q \in RT_0(\mathcal{T}) \\ q \cdot \nu|_{\partial\Omega} = (\gamma_{\mathrm{t}}(\nabla u_D))_{\mathcal{E}(\Omega)}}} \left(C_F \left\| \operatorname{div} q \right\|_{L^2(\Omega)} + \left\| \varkappa^{1/2}(q_{\mathrm{Repin}} - \operatorname{Curl}_{\mathrm{NC}} u_{\mathrm{CR}}) \right\|_{L^2(\Omega)} \right),
$$

with Friedrichs' constant $C_F := \sup_{v \in V \backslash \{0\}} \left\| v \right\|_{L^2(\Omega)} / \|v\|$ (or any upper bound of it). See [Val09] for details on the following algorithm for the computation of q_{LS}. For any $\beta > 0$, the Young inequality yields

$$
\begin{aligned}
& \left(\left\| \varkappa^{1/2}(q_{\mathrm{Repin}} - \operatorname{Curl}_{\mathrm{NC}} u_{\mathrm{CR}}) \right\|_{L^2(\Omega)} + C_F \left\| \operatorname{div} q \right\|_{L^2(\Omega)} \right)^2 \\
& \leqslant (1 + \beta) \left\| \varkappa^{1/2}(q_{\mathrm{Repin}} - \operatorname{Curl}_{\mathrm{NC}} u_{\mathrm{CR}}) \right\|_{L^2(\Omega)}^2 + C_F^2(1 + 1/\beta) \left\| \operatorname{div} q \right\|_{L^2(\Omega)}^2 =: \mathcal{M}(\beta, q).
\end{aligned}
$$

Therefore,

$$
\| \operatorname{Res}_{NC} \|_\star \leqslant \min_{0 < \beta} \min_{q \in H(\operatorname{div}, \Omega)} \mathcal{M}(\beta, q)^{1/2}
$$

and we now have to minimise the quadratic functional $\mathcal{M}(\beta, q)$. For some fixed q the optimal choice for β is

$$
(6.3) \qquad \beta = \frac{C_F \left\| \operatorname{div} q \right\|_{L^2(\Omega)}}{\left\| \varkappa^{1/2}(q_{\mathrm{Repin}} - \operatorname{Curl}_{\mathrm{NC}} u_{\mathrm{CR}}) \right\|_{L^2(\Omega)}}.
$$

Given an initial $\beta > 0$, compute the optimal $q_\beta \in RT_0(\mathcal{T})$. Then, use (6.3) to update β for the next minimisation of q_β. After three iterations we arrive at (some very good approximation

of) q_{Repin}. The estimator reads

$$\eta_{\mathrm{Repin}}^2 := \eta^2 + \big(C_F \big\|\varkappa^{1/2}\operatorname{div} q_{\mathrm{Repin}}\big\|_{L^2(\Omega)} + \big\|\varkappa^{1/2}(q_{\mathrm{Repin}} - \operatorname{Curl}_{\mathrm{NC}} u_{\mathrm{CR}})\big\|_{L^2(\Omega)}$$
$$+ C_2 \operatorname{osc}(\varkappa^{1/2}\gamma_{\mathrm{t}}(\nabla u_D), \mathcal{E}(\partial\Omega))\big)^2.$$

The η_{Repin}-driven ACRFEM algorithm in Subsection 2.4 replaces $\eta_{\mathrm{R}}(T)^2$ by

$$\eta_{\mathrm{Repin}}(T)^2 := \big\|\varkappa^{-1/2}f_{\mathcal{T}}/d\ (\bullet - \operatorname{mid}(\mathcal{T}))\big\|_{L^2(T)}^2 + h_T^2/\pi^2 \big\|\varkappa^{-1/2}(f - f_{\mathcal{T}})\big\|_{L^2(T)}^2$$
$$+ C_F^2 \big\|\operatorname{div} q_{\mathrm{Repin}}\big\|_{L^2(T)}^2 + \big\|\varkappa^{1/2}(q_{\mathrm{Repin}} - \operatorname{Curl}_{\mathrm{NC}} u_{\mathrm{CR}})\big\|_{L^2(T)}^2$$
$$+ C_2^2 \operatorname{osc}(\varkappa^{1/2}\gamma_{\mathrm{t}}(\nabla u_D), \mathcal{E}(T) \cap \mathcal{E}(\partial\Omega))^2.$$

6.5. Localisation after Carstensen and Funken.
The partition of unity property of the nodal basis functions yields the residual split

$$\operatorname{Res}_{\mathrm{NC}}(v) = \sum_{z \in \mathcal{N}} \operatorname{Res}_{\mathrm{NC}}(\varphi_z v)$$

and since $\operatorname{Res}_{\mathrm{NC}}(\varphi_z) = 0$ for $z \in \mathcal{N}$ there exists an unique solution $w_z \in W_z := \big\{v \in H^1_{\mathrm{loc}}(\omega_z) \,\big|\, \big\|\varkappa^{-1/2}\varphi_z^{1/2}\nabla v\big\|_{L^2(\omega_z)} < \infty\big\}/\mathbb{R}$ such that

$$(6.4) \qquad \int_{\omega_z} \varphi_z(\varkappa^{-1}\nabla\omega_z) \cdot \nabla v\, dx = \operatorname{Res}_{\mathrm{NC}}(\varphi_z v) \quad \text{for all } v \in W_z.$$

It holds (see [CF99])

$$\|\operatorname{Res}_{NC}\|_\star \leqslant \left(\sum_{z \in \mathcal{N}} \big\|\varkappa^{-1/2}\varphi_z^{1/2}\nabla w_z\big\|_{L^2(\omega_z)}^2\right)^{1/2}.$$

In the actual computations, the local problems (6.4) are solved with fourth-order polynomials. The final error estimator reads

$$\eta_{\mathrm{CF}}^2 := \eta^2 + \sum_{z \in \mathcal{N}} \big\|\varkappa^{-1/2}\varphi_z^{1/2}\nabla w_z\big\|_{L^2(\omega_z)}^2.$$

The η_{CF}-driven ACRFEM algorithm in Subsection 2.4 replaces $\eta_{\mathrm{R}}(T)^2$ by

$$\eta_{\mathrm{CF}}(T)^2 := \big\|\varkappa^{-1/2}f_{\mathcal{T}}/d\ (\bullet - \operatorname{mid}(\mathcal{T}))\big\|_{L^2(T)}^2 + h_T^2/\pi^2 \big\|\varkappa^{-1/2}(f - f_{\mathcal{T}})\big\|_{L^2(T)}^2$$
$$+ 1/3 \sum_{z \in \mathcal{N}(T)} \big\|\varkappa^{-1/2}\varphi_z^{1/2}\nabla w_z\big\|_{L^2(\omega_z)}^2.$$

6.6. Link between interpolation and equilibration.
The interpolation error estimators from Section 4 design piecewise polynomial interpolations $v \in P_1(\widehat{\mathcal{T}}) \cap C(\Omega)$ of u_{CR}. However, the rotation of their gradients ∇v results in some divergence-free $q := \operatorname{Curl} v \in RT_0(\widehat{\mathcal{T}})$ with

$$\|u_{\mathrm{CR}} - v\|_{\mathrm{NC}} = \big\|\varkappa^{1/2}(\operatorname{Curl}_{\mathrm{NC}} u_{\mathrm{CR}} - \operatorname{Curl} v)\big\|_{L^2(\Omega)}.$$

The arguments of Subsection 6.1 on equilibration techniques apply to the aforementioned q and result in Theorem 6.1 which is equivalent to the outcome from Theorem 3.1.b for homogeneous Dirichlet data. This explains the comparable performance of η_{A} and η_{B} in the numerical experiments of Section 7.

6.7. **Further postprocessing.** Some postprocessing in the spirit of [CMx3] simply replaces q in (6.1) by $q + \mathrm{Curl}\, w$ for any $w \in H_0^1(\Omega)$. Since $\mathrm{Curl}\, w$ is zero along the boundary and has zero divergence, Theorem 6.1 immediately leads to

$$\| \mathrm{Res}_{\mathrm{NC}} \|_\star \leqslant C_F \big\| \varkappa^{1/2} \operatorname{div} q \big\|_{L^2(\Omega)} + \big\| \varkappa^{1/2}(q - \mathrm{Curl}_{\mathrm{NC}}\, u_{\mathrm{CR}} - \mathrm{Curl}\, w) \big\|_{L^2(\Omega)}$$
$$+ C_2 \big\| (h_{\mathcal{E}} \varkappa)^{1/2}(\gamma_{\mathrm{t}}(\nabla u_D) - q \cdot \nu) \big\|_{L^2(\partial\Omega)}.$$

The design of w employs the red-refinement $\widehat{\mathcal{T}} := \mathrm{red}(\mathcal{T})$ (or the dual mesh $\widehat{\mathcal{T}} := \mathcal{T}^\star$ in case of q_{LW}) and approximates

$$\operatorname{argmin}_{w \in P_1(\widehat{\mathcal{T}}) \cap C(\Omega)/\mathbb{R}} \big\| \varkappa^{1/2}(q - \mathrm{Curl}_{\mathrm{NC}}\, u_{\mathrm{CR}} - \mathrm{Curl}\, w) \big\|_{L^2(\Omega)}.$$

Following our experiences from [CMx3], we use a Jacobi-preconditioned cg scheme with initial value 0 and stop after one single iteration. This defines some $w^{(1)}$ and

$$\eta^2_{\mathrm{xyz}(r,1)} := \eta^2 + \Big(\big\| \varkappa^{1/2}(q_{\mathrm{xyz}} - \mathrm{Curl}_{\mathrm{NC}}\, u_{\mathrm{CR}} - \mathrm{Curl}\, w^{(1)}) \big\|_{L^2(\Omega)} + \eta_{\mathrm{Db}} \Big)^2$$

(with some non-changing contribution η_{Db} that reflects the influence of the inhomogeneous boundary conditions) or, for $\widehat{\mathcal{T}} = \mathcal{T}^\star$,

$$\eta^2_{\mathrm{LW}(1)} := \eta^2 + \big(\big\| \varkappa^{1/2}(q_{\mathrm{LW}} - \mathrm{Curl}_{\mathrm{NC}}\, u_{\mathrm{CR}} - \mathrm{Curl}\, w^{(1)}) \big\|_{L^2(\Omega)}$$
$$+ C_2 \big\| (h_{\mathcal{E}} \varkappa)^{1/2}(\gamma_{\mathrm{t}}(\nabla u_D) - q_{\mathrm{LW}} \cdot \nu) \big\|_{L^2(\partial\Omega)} \big)^2.$$

Since the quantity $q = \mathrm{Curl}\, v_{\mathrm{MP1RED}(\infty)}$ is already the best-approximation amongst $\mathrm{Curl}\big(P_1(\mathrm{red}(\mathcal{T})) \cap C(\Omega) \big)$, $\eta_{\mathrm{MP1RED}(\infty)}$ acts as a lower bound for all postprocessed quantities based on $q \in RT_0(\mathrm{red}(\mathcal{T}))$ and $\widehat{\mathcal{T}} = \mathrm{red}(\mathcal{T})$. Of course, more red-refinements lead to better accuracy but also more costly computations.

7. Numerical Experiments

This section is devoted to some numerical experiments to report on the efficiency of the estimators in the benchmark examples from Table 1.

7.1. **Numerical example on L-shaped domain with corner singularity.** The first benchmark problem employs $f \equiv 0$, $\varkappa \equiv 1$ and inhomogeneous Dirichlet data u_D given by the exact solution

$$u(r, \varphi) = r^{2/3} \sin(2\varphi/3)$$

on the L-shaped domain $\Omega = (-1,1)^2 \setminus ([0,1] \times [-1,0])$. The problem involves a typical corner singularity and shows an empirical convergence rate of $1/3$ related to the degrees of freedom for uniform mesh refinement. Since the source term is zero, the overhead contribution η of the estimator vanishes. Adaptive mesh refinement with any described estimators improves the convergence rate to the optimal value 0.5 (see Figure 7.3). Figures 7.1 and 7.2 compare the efficiency indices of all estimators for uniform and adaptive mesh refinement, respectively. The efficiency indices vary between 1.1 for η_{MP2} and 1.6 for η_{A} and η_{B}. The improved estimators $\eta_{\mathrm{MP1RED}(0)}$ and η_{PMRED} perform slightly better than η_{A} for uniform mesh refinement, but significantly better for adaptive mesh refinement. Here, the overestimation decreases under 35 percent which is even better than η_{MP1} or η_{Repin}. The estimator η_{LW} performs similar but slightly worse compared to $\eta_{\mathrm{MP1RED}(0)}$. The efficiency of the error estimator η_{AP2} is even comparable to the postprocessed quantities $\eta_{\mathrm{Repin}(r,1)}$, $\eta_{\mathrm{A}(r,1)}$ or $\eta_{\mathrm{B}(r,1)}$ for adaptive mesh refinement.
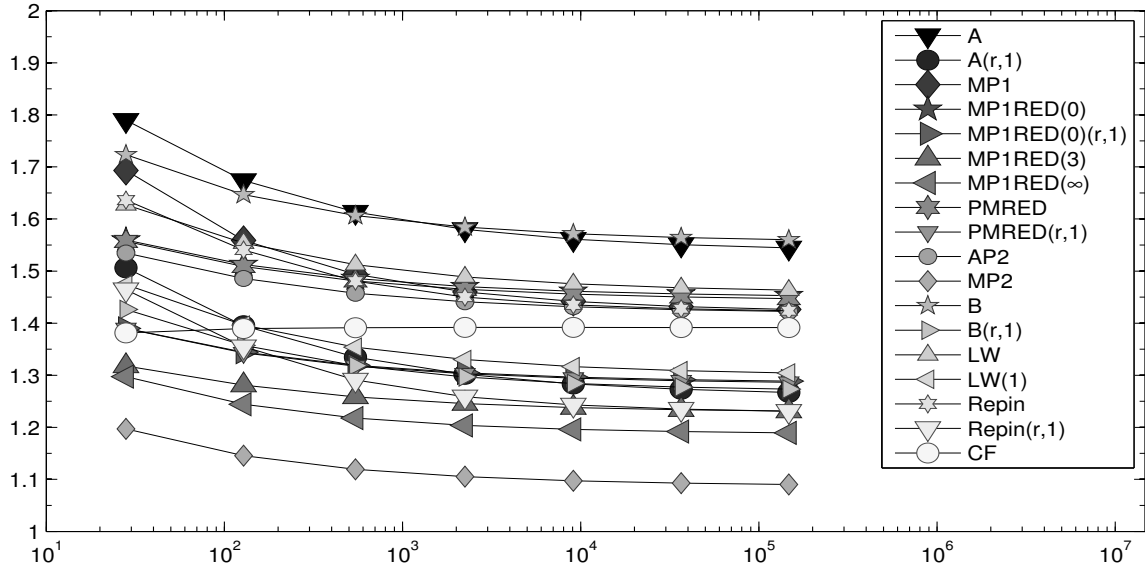
FIGURE 7.1. History of efficiency indices $\eta_{\mathrm{xyz}}/\|e\|_{\mathrm{NC}}$ of various a posteriori error estimators η_{xyz} labelled xyz in the figure as functions of the number of unknowns on uniform meshes in Subsection 7.1.
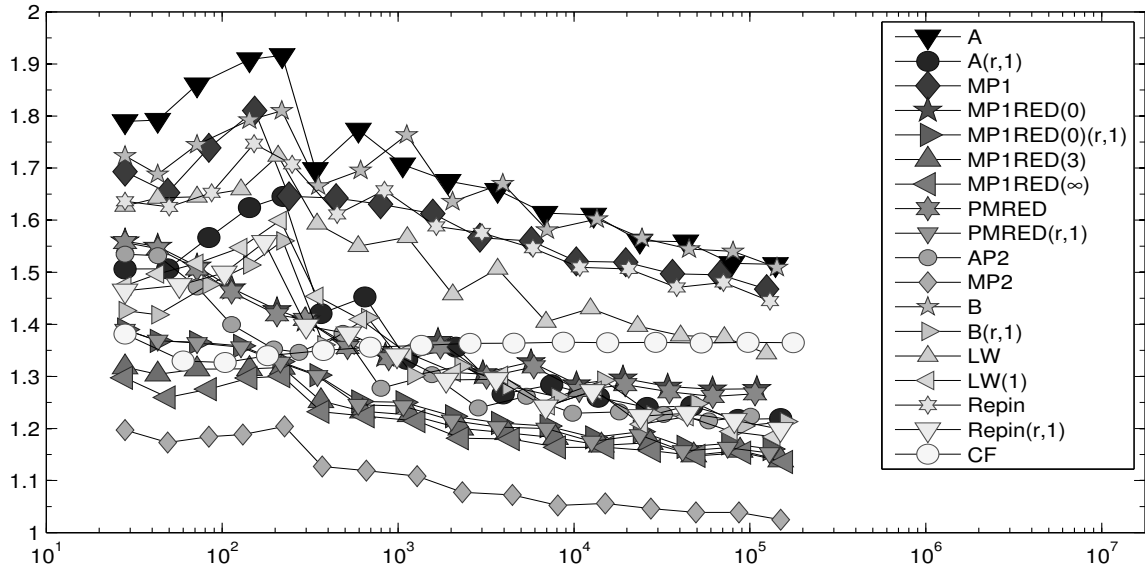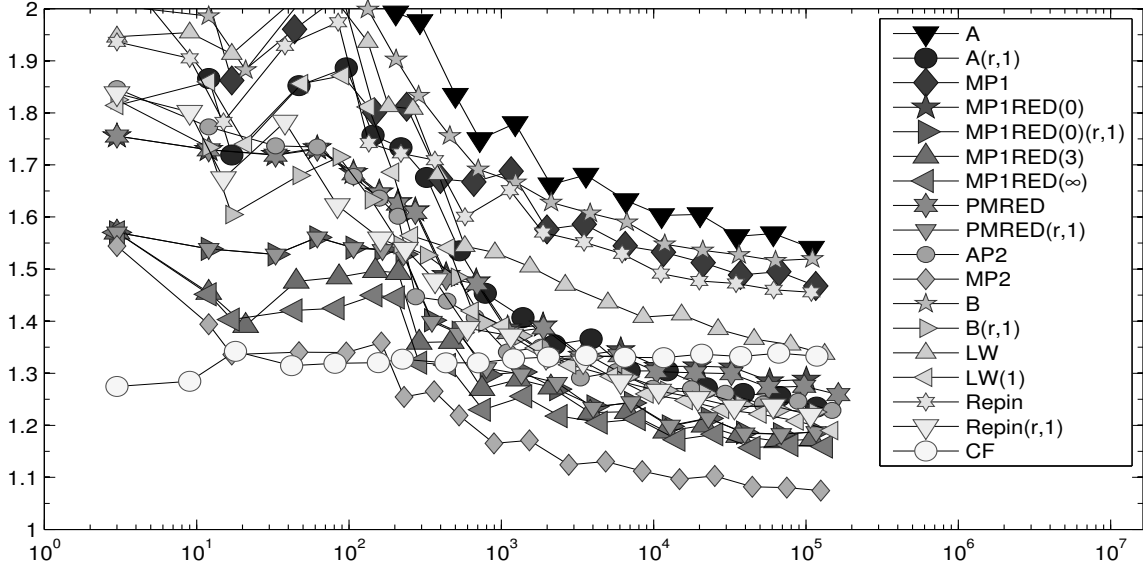

FIGURE 7.2. History of efficiency indices $\eta_{\mathrm{xyz}}/\|e\|_{\mathrm{NC}}$ of various a posteriori error estimators η_{xyz} labelled xyz in the figure as functions of the number of unknowns on adaptive meshes in Subsection 7.1.

7.2. Numerical example on slit domain with slit singularity.

Our second benchmark problem employs $f \equiv 1$, $\varkappa \equiv 1$ and u_D matching the exact solution $u(r, \varphi) = r^{1/2} \sin(\varphi/2) - (1/2)(r \sin(\varphi))^2$ on the slit domain

$$\Omega = \{(x, y) \in \mathbb{R}^2 \,\big|\, |x| + |y| < 1\} \backslash ([0, 1] \times \{0\}).$$
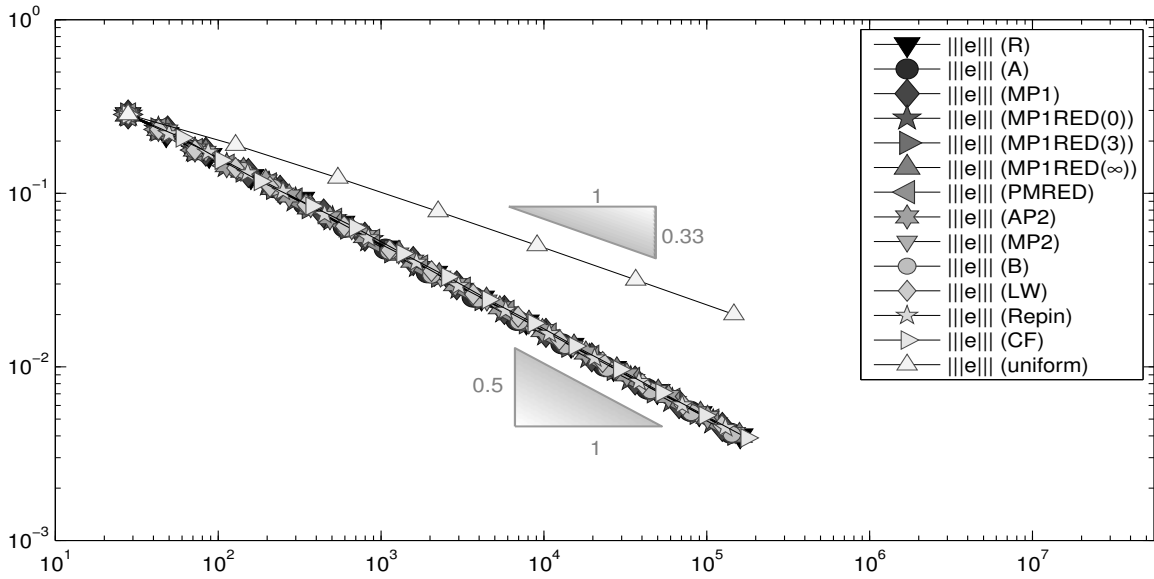
FIGURE 7.3. Convergence history of the energy error for uniform and adaptive mesh-refinements in Subsection 7.1.

Figures 7.4 and 7.5 show similar efficiency histories of the estimators as in the first Example. The large pre-asymptotic range of the efficiency indices of some estimators indicate an influence of the oscillations of the inhomogeneous boundary data. Estimator like η_{MP2}, η_{MP1RED}, $\eta_{\mathrm{MP1RED(0)}}$ or η_{PMRED} with more degrees of freedom along $\partial\Omega$ (due to the employment of $P_1(\mathrm{red}(\mathcal{T}))$ or $P_2(\mathcal{T})$ elements) are less affected by these oscillations. The proportion $\eta/\|e\|_{\mathrm{NC}}$ decreases from 30 percent on the initial triangulation to below 3 percent. Hence, the overhead term does not dominate the upper bound.
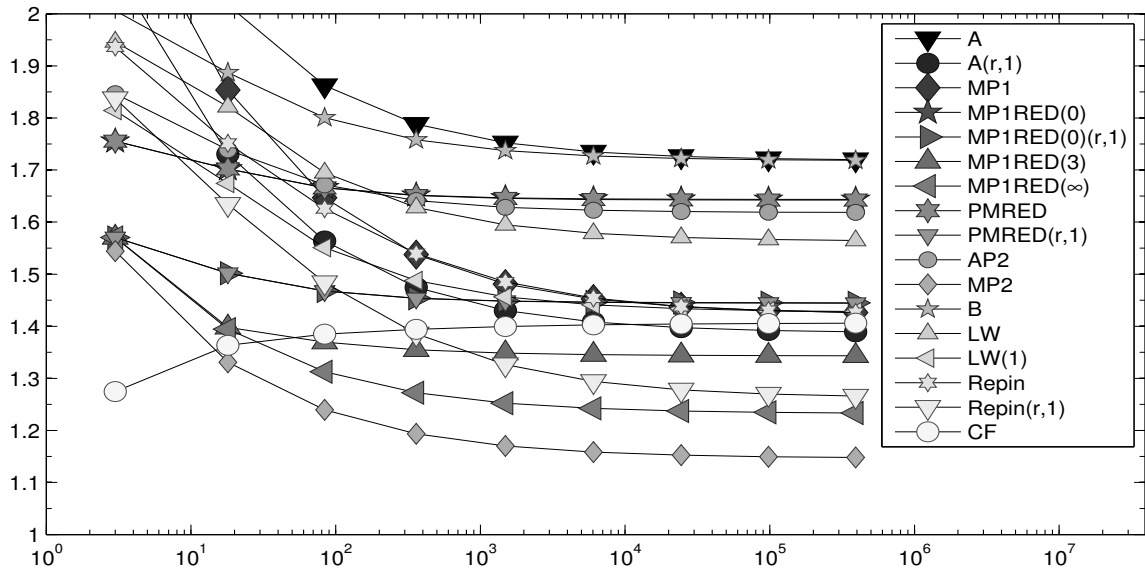
FIGURE 7.4. History of efficiency indices $\eta_{\mathrm{xyz}}/\|e\|_{\mathrm{NC}}$ of various a posteriori error estimators η_{xyz} labelled xyz in the figure as functions of the number of unknowns on uniform meshes in Subsection 7.2.

FIGURE 7.5. History of efficiency indices $\eta_{\mathrm{xyz}}/\|\!|e|\!\|_{\mathrm{NC}}$ of various a posteriori error estimators η_{xyz} labelled xyz in the figure as functions of the number of unknowns on adaptive meshes in Subsection 7.2.

7.3. **Numerical example on square domain with oscillations** [LW04]**.** The third benchmark problem employs homogeneous boundary data $u_D \equiv 0$, $\varkappa \equiv 1$, and an oscillating source term f that matches the exact solution $u(x,y) = x(x-1)y(y-1)\exp(-100(x-1/2)^2 - 100(y-117/1000)^2)$ on the square domain $\Omega = (0,1)^2$. Since the solution is smooth, there is no improvement of the convergence rate by adaptive mesh refinement, but there is a significant reduction of the pre-asymptotic range. The overall efficiency of all estimators is very good (below 1.5) and similar for uniform and adaptive mesh refinement, see Figures 7.6 and 7.7. Our improved estimator $\eta_{\mathrm{MP1RED}(0)}$ and η_{PMRED} perform better than η_{AP2}, η_{LW} and η_{A} which is already quite optimal in comparison with η_{MP1}. The influence of the overhead term η is more significant than in the other examples before, $\eta/\|\!|e|\!\|_{\mathrm{NC}}$ arrives at values around 0.6. However, the other contribution $\left\| \nabla_{\mathrm{NC}} u_{\mathrm{CR}} - \nabla v_{\mathrm{xyz}} \right\|_{L^2(\Omega)}$ is still crucial for the sharpness of the upper bound.

7.4. **Numerical example on 3/4-disk domain with corner singularity** [Ain04]**.** The fourth problem employs $u_D \equiv 0$ and f matching the exact solution $u(r,\varphi) = (r^{2/3} - r^2)\sin(2\varphi/3)$ on the sector domain

$$\Omega = \{x = (r\cos\varphi, r\sin\varphi) \in B(0,1) \,\big|\, \varphi \in [0, 3\pi/2]\}.$$

As in the L-shape example from Subsection 7.1, we have a singularity due to a reentrant corner. Since the domain is not matched exactly, $\bigcup\mathcal{T} \subset \overline{\Omega}$ requires extra considerations for u_{CR} extended by zero outside of $\bigcup\mathcal{T}$ such that $u_{\mathrm{CR}} = 0$ along $\partial\Omega$. The reflection of boundary triangles of Figure 7.8 yields an extended triangulation $\widehat{\mathcal{T}}$ with $\Omega \subset \bigcup\widehat{\mathcal{T}}$. The new triangles involve only Dirichlet nodes and so the design of v from Section 4 on $\mathcal{T}$ or $\mathrm{red}(\mathcal{T})$ can be extended $H^1(\Omega)$-conformly by $v_{\mathrm{xyz}} = 0$ on $\widehat{\mathcal{T}}\backslash\mathcal{T}$ or $\mathrm{red}(\widehat{\mathcal{T}}\backslash\mathcal{T})$. Since the normal fluxes of q are zero along $\partial\bigcup\mathcal{T}$ for any design from Section 6, also q can be extended
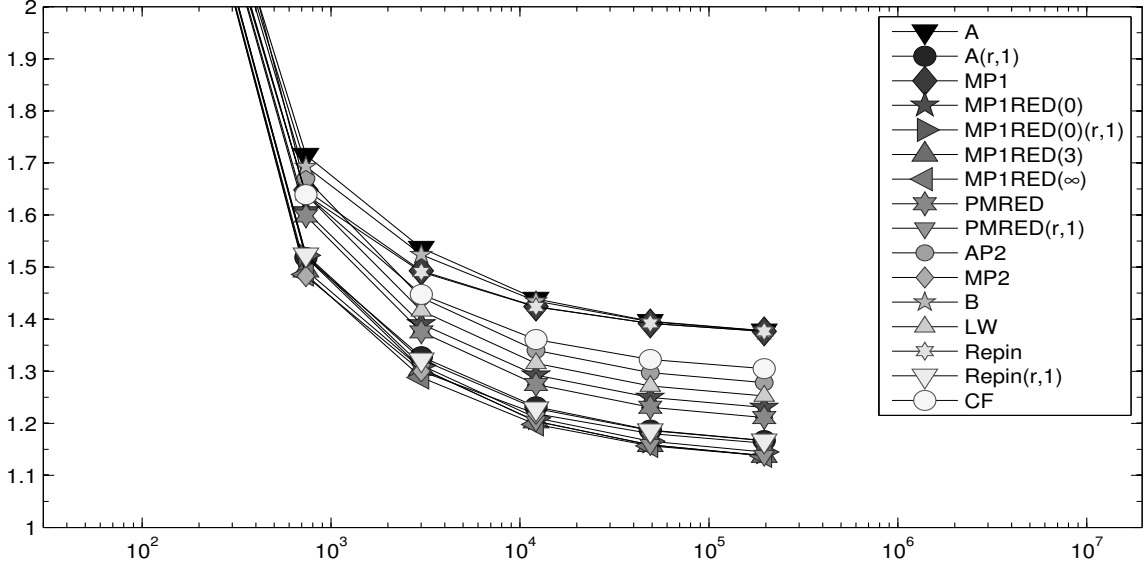
FIGURE 7.6. History of efficiency indices $\eta_{\mathrm{xyz}}/\|e\|_{\mathrm{NC}}$ of various a posteriori error estimators η_{xyz} labelled xyz in the figure as functions of the number of unknowns on uniform meshes in Subsection 7.3.
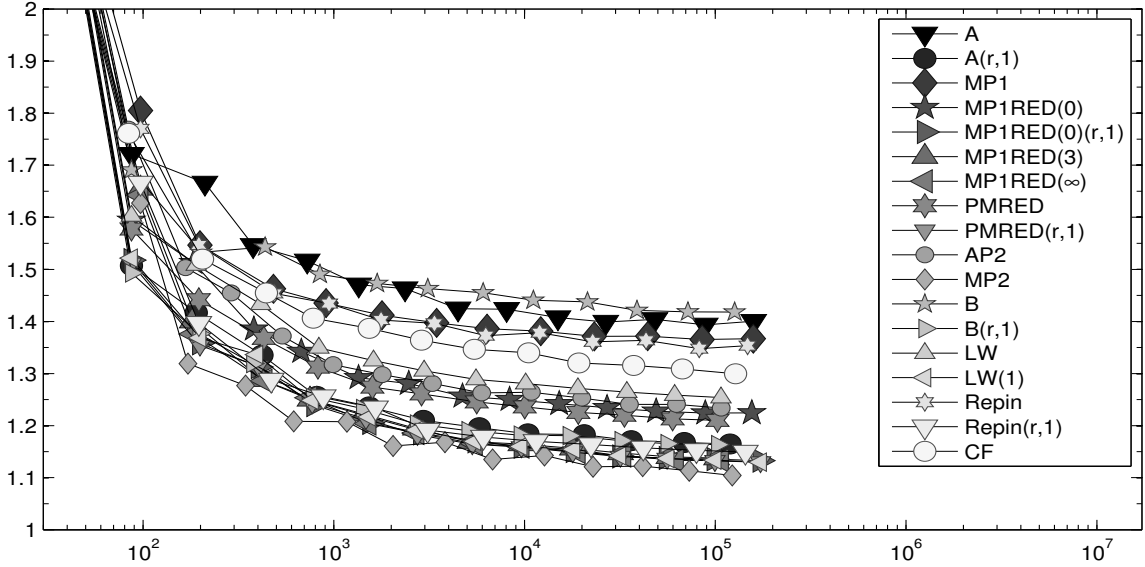

FIGURE 7.7. History of efficiency indices $\eta_{\mathrm{xyz}}/\|e\|_{\mathrm{NC}}$ of various a posteriori error estimators η_{xyz} labelled xyz in the figure as functions of the number of unknowns on adaptive meshes in Subsection 7.3.

$H(\mathrm{div}, \Omega)$-conformly by $q_{\mathrm{xyz}} = 0$ on $\widehat{\mathcal{T}} \backslash \mathcal{T}$. This leads to the guaranteed upper bound

$$(7.1) \qquad \|e\|_{\mathrm{NC}}^2 \leqslant \left(\left\| \varkappa^{-1/2} f_{\widehat{\mathcal{T}}}/d \left(\bullet - \mathrm{mid}(\widehat{\mathcal{T}}) \right) \right\|_{L^2(\bigcup \widehat{\mathcal{T}})} + \mathrm{osc}(\varkappa^{-1/2} f, \widehat{\mathcal{T}})/\pi \right)^2 + \mu_{\mathrm{xyz}}^2.$$

For simplicity, the overhead term η in (7.1) is calculated on $\bigcup \widehat{\mathcal{T}}$ instead on Ω. This may result in some unnecessary overestimation on coarse meshes, but the effect decreases with
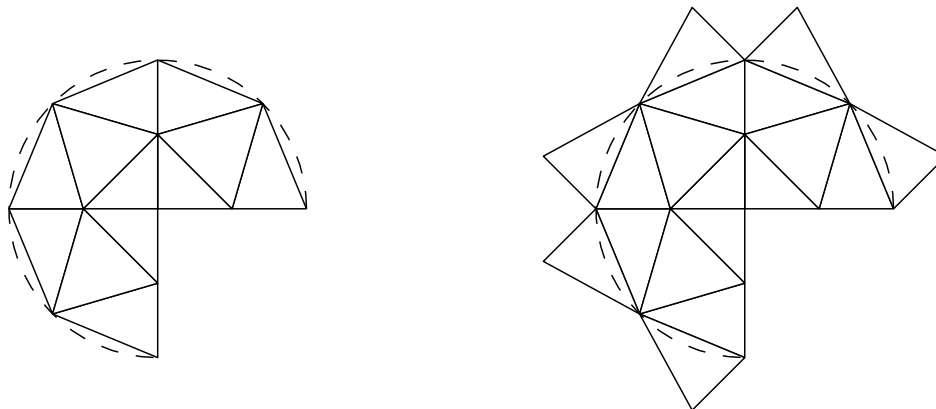
FIGURE 7.8. Triangulation $\mathcal{T}$ (left, solid lines) and extended triangulation $\widehat{\mathcal{T}}$ (right, solid lines) with $\bigcup \mathcal{T} \subseteq \Omega \subseteq \bigcup \widehat{\mathcal{T}}$ for the sector domain Ω (dashed lines) from Section 7.4.

an increasing number of degrees of freedom. Qualitatively the performance of the error estimators is similar to the first examples.
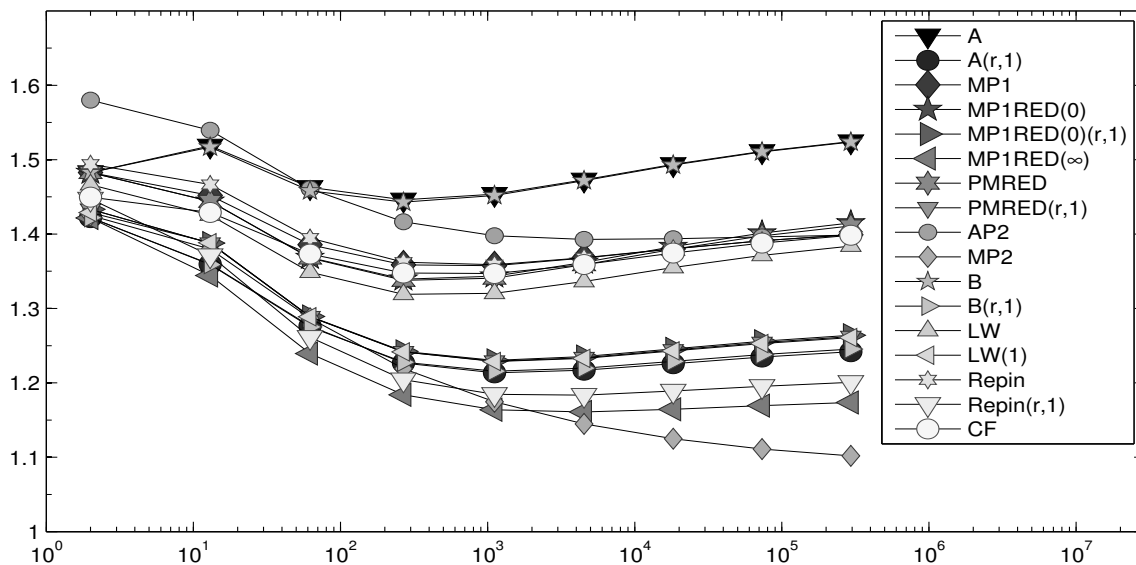

FIGURE 7.9. History of efficiency indices $\eta_{\mathrm{xyz}}/\|e\|_{\mathrm{NC}}$ of various a posteriori error estimators η_{xyz} labelled xyz in the figure as functions of the number of unknowns on uniform meshes in Subsection 7.4.

7.5. **Numerical example on square domain with discontinuous diffusion** [Ain04]. Our fifth benchmark involves $f \equiv 0$ and u_D matches the exact quadratic function $u(x,y) = (x^2 - y^2)/\varkappa$ on the square domain $\Omega = (-1,1)^2$. The diffusion parameter $\varkappa$ assumes the values $1, 100, 10000$ on subdomains depicted in Figure 7.11. Since $u \in P_2(\mathcal{T}) \cap C(\Omega)$, the error estimator η_{MP2} is almost exact as depicted in Figures 7.12 and 7.13. There is only a
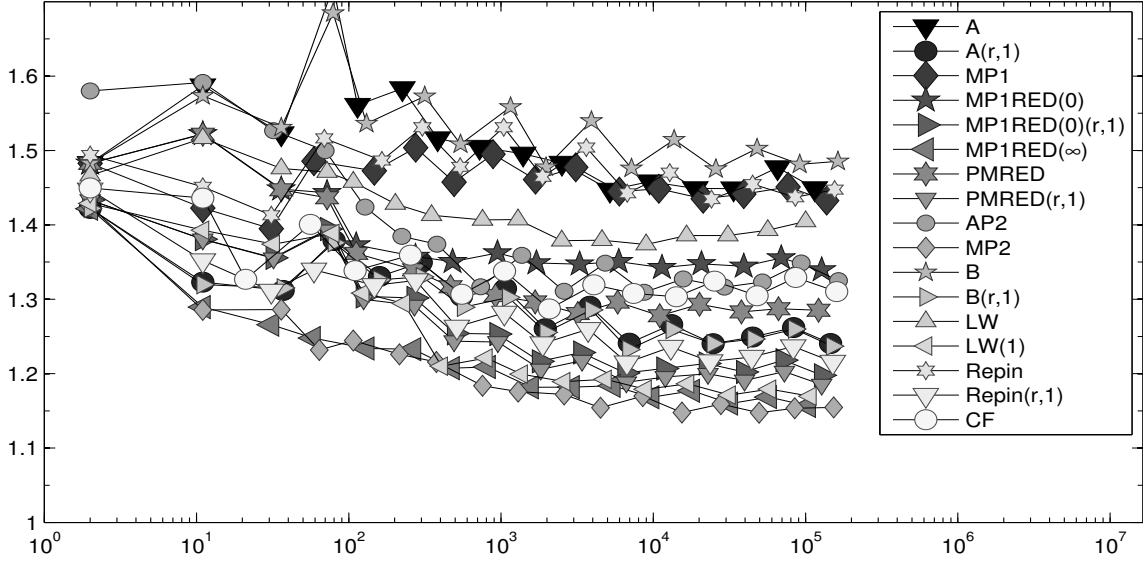
FIGURE 7.10.   History of efficiency indices $\eta_{\mathrm{xyz}}/\|e\|_{\mathrm{NC}}$ of various a posteriori error estimators η_{xyz} labelled xyz in the figure as functions of the number of unknowns on adaptive meshes in Subsection 7.4.
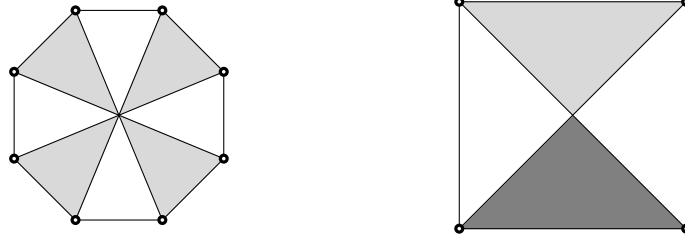

FIGURE 7.11. Distribution of $\varkappa = 1$ (white) and $\varkappa = 1000$ (lightgray) in octagon domain of Subsection 7.6 (left) and distribution of $\varkappa = 1$ (white), $\varkappa = 100$ (lightgray) and $\varkappa = 10000$ (darkgray) in square domain of Subsection 7.5.

small reliability-effiency gap due to the inhomogeneous boundary conditions. The two equilibration error estimator η_{B} and η_{A} show extremely large efficiency gaps on coarse meshes. Additionally, Figure 7.14 shows that the adaptive mesh-refinement by η_{R}, η_{B} and $\eta - \mathrm{LW}$ on coarse meshes is slightly worse in the beginning. These effects are possibly related to the jumps in the diffusion coefficients. All other error estimators perform similar as in the previous experiments with $\varkappa \equiv 1$, but in this example η_{AP2} is very close to the optimal η_{MP2}.

7.6. Numerical example on octagon domain with discontinuous diffusion [HHW96].
The last benchmark problem employs $f \equiv 0$ and u_D matching the exact solution $u(x,y) = ((ax^2 - y^2)(ay^2 - x^2))/\varkappa$ with $a = \tan((3\pi)/8)^2$ on the oktagon domain

$$\Omega = \mathrm{conv}\left\{(\cos((2j+1)\pi/8), \sin((2j+1)\pi/8)), \; j = 0, 1, .., 7\right\}.$$

The diffusion coefficients $\varkappa$ take alternately the values 1 and 1000 as depicted in Figure 7.11. The results from Figure 7.15 and 7.16 are similar to the results from Subsection 7.6.
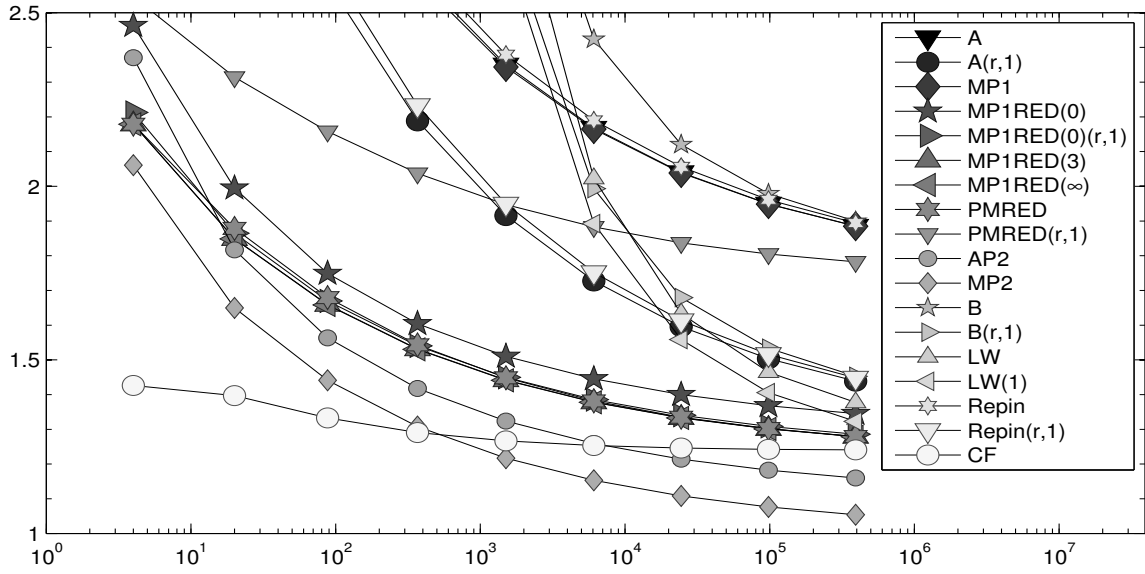
FIGURE 7.12.   History of efficiency indices $\eta_{\mathrm{xyz}}/\|e\|_{\mathrm{NC}}$ of various a posteriori error estimators η_{xyz} labelled xyz in the figure as functions of the number of unknowns on uniform meshes in Subsection 7.5.
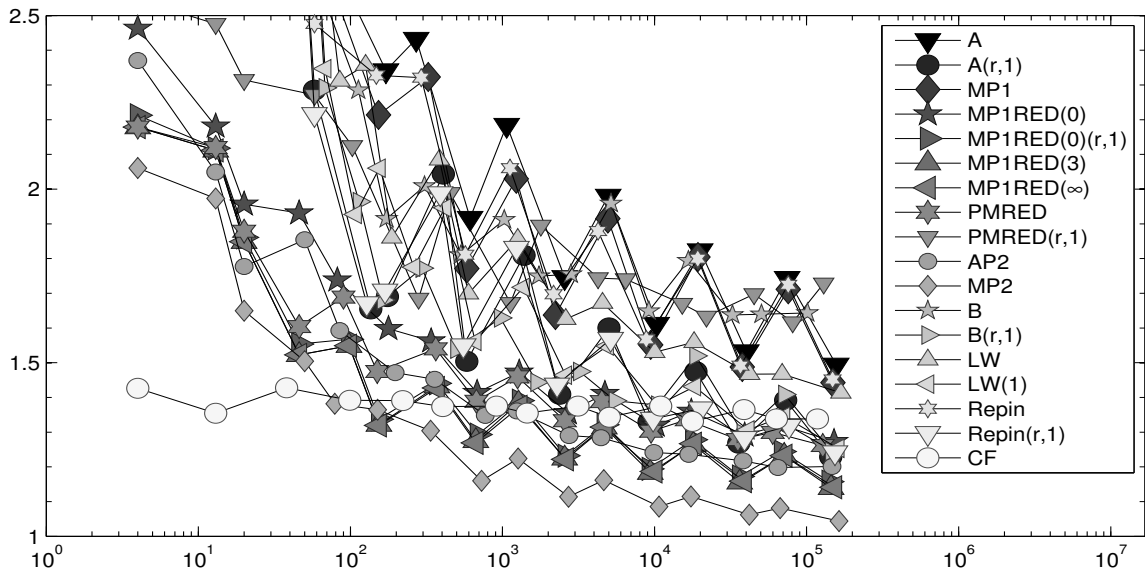

FIGURE 7.13.   History of efficiency indices $\eta_{\mathrm{xyz}}/\|e\|_{\mathrm{NC}}$ of various a posteriori error estimators η_{xyz} labelled xyz in the figure as functions of the number of unknowns on adaptive meshes in Subsection 7.5.
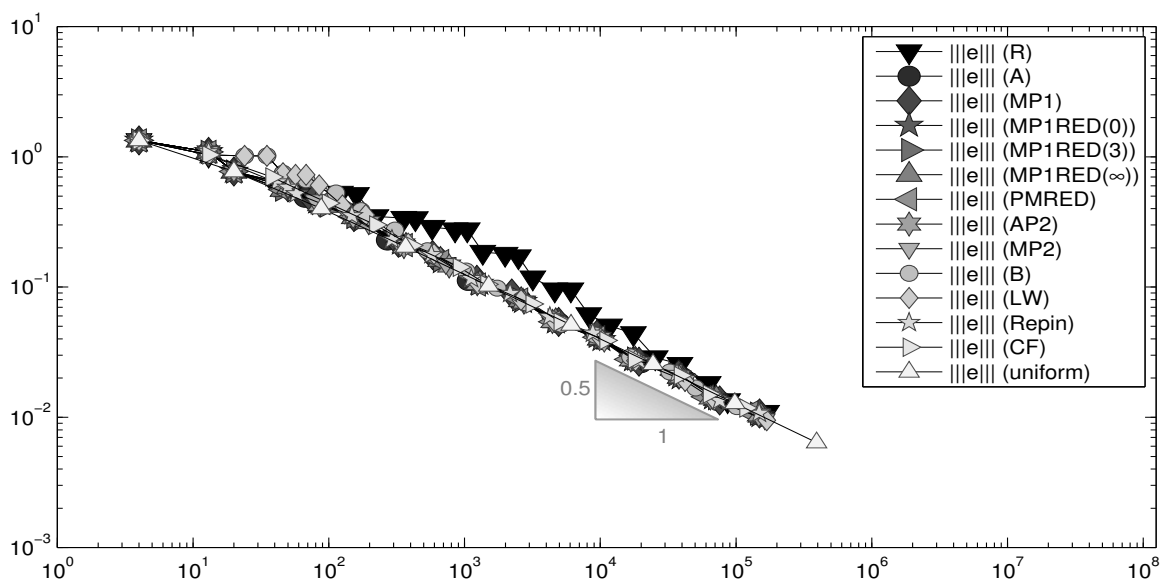
FIGURE 7.14. Convergence history of the energy error for uniform and adaptive mesh-refinements in Subsection 7.5.
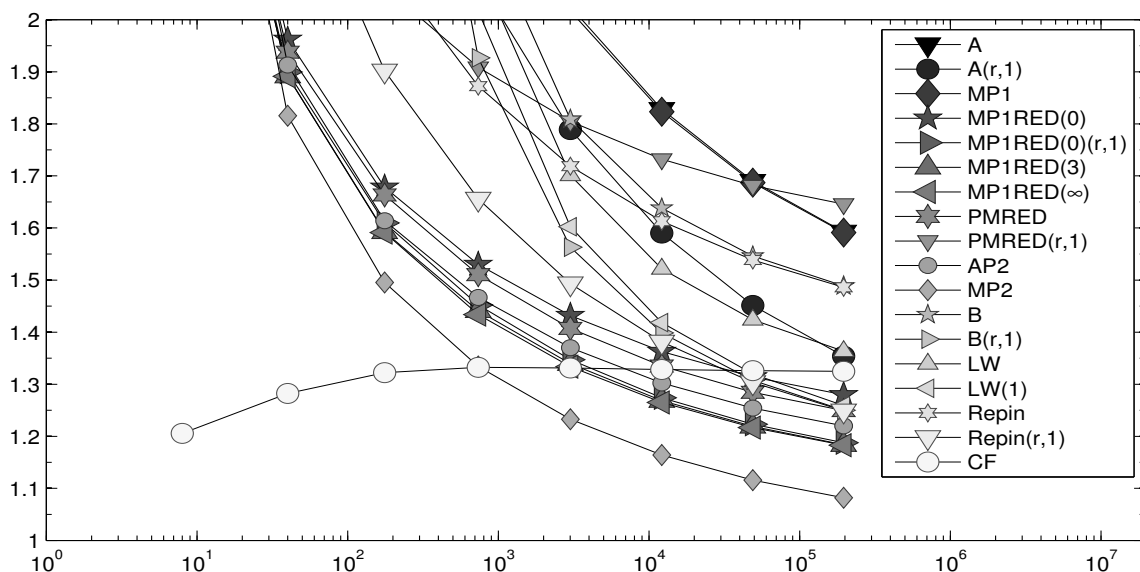

FIGURE 7.15. History of efficiency indices $\eta_{\mathrm{xyz}}/\|e\|_{\mathrm{NC}}$ of various a posteriori error estimators η_{xyz} labelled xyz in the figure as functions of the number of unknowns on uniform meshes in Subsection 7.6.

8. Remarks and Conclusions

8.1. **On improved interpolation operators.** The novel interpolation $v_{\mathrm{MP1RED}(0)}$ from Subsection 4.2 performs far better than v_{A} in all numerical experiments of Section 7, especially in problems with jumping diffusion coefficients (Subsections 7.5 and 7.6) and all examples with adaptive mesh refinement. The further improvement of $v_{\mathrm{MP1RED}(0)}$ by v_{PMRED} is significant and its efficiency is is comparable to that of η_{AP2} in most examples.
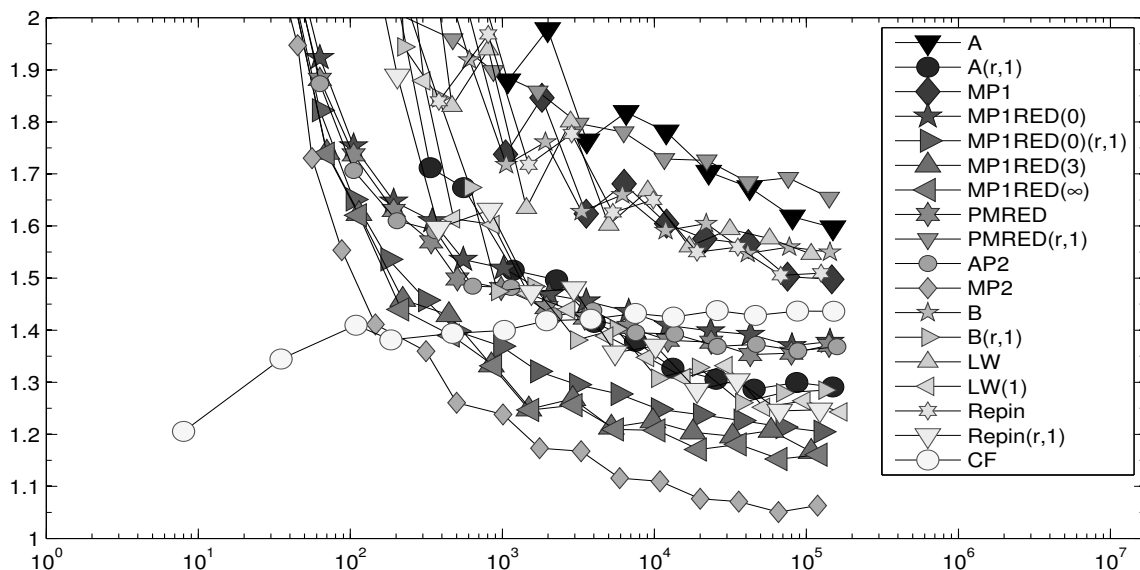
FIGURE 7.16.   History of efficiency indices $\eta_{\mathrm{xyz}}/\|\!|e|\!\|_{\mathrm{NC}}$ of various a posteriori error estimators η_{xyz} labelled xyz in the figure as functions of the number of unknowns on adaptive meshes in Subsection 7.6.

8.2. **On global minimisation.** The optimal estimators η_{MP1}, η_{MP1RED} and η_{MP2} involve the solution of high-dimensional linear systems of equations. The truncated iterative solve via a preconditioned conjugate gradients scheme based on the initial value $v_{\mathrm{MP1RED(0)}}$ of Subsection 4.2 leads to $\eta_{\mathrm{MP1RED(3)}}$. The truncation after three iterations is highly efficient in Subsections 7.1-7.4, but not for the examples with jumping coefficients of Subsections 7.5-7.6. The P_2 interpolation v_{AP2} allows a very efficient estimator but with a large gap to the optimal P_2 function v_{MP2}. This may motivate its use for an initial value for some iterative approximation of v_{MP2}.

8.3. **On other error estimators.** Equilibration or localisation techniques after [LW04, Rep08, CF99] lead to accurate error control with efficiency indices between those of η_{A} and $\eta_{\mathrm{MP1RED(0)}}$ in most examples of Section 7. The overhead term η neither dominates the upper bound nor pollutes the efficiency of the sharper estimators like η_{MP2}.

8.4. **On postprocessing.** The postprocessing of Subsection 6.7 leads to more accurate error estimators which are competitive even with $\eta_{\mathrm{MP1RED(\infty)}}$.

8.5. **On adaptive mesh refinement.** The steering of the adaptive mesh refinements can be based on each of the 11 estimators from Table 2. In all numerical examples the convergence of the error in the energy norm is quite comparable for all these cases. There is no particular strategy of superior convergence — any of η_{A}, $\eta_{\mathrm{MP1RED(0)}}$, η_{PMRED}, ... will do. For discontinuous coefficients, the equilibration error estimators η_{B} and η_{LW} and the residual-based error estimator η_{R} lead to slightly worse results than the other error estimators on coarse meshes.

References

[Ago94] A. Agouzal, *A posteriori error estimator for nonconforming finite element methods*, Appl. Math. Lett. **7** (1994), no. 5, 61–66.

[Ain08] Mark Ainsworth, *A posteriori error estimation for lowest order Raviart-Thomas mixed finite elements*, SIAM J. Sci. Comput. **30** (2007/08), no. 1, 189–204.

[Ain04] _____, *Robust a posteriori error estimation for nonconforming finite element approximation*, SIAM J. Numer. Anal. **42** (2004), no. 6, 2320–2341.

[AO00] M. Ainsworth and J. T. Oden, *A Posteriori Error Estimation in Finite Element Analysis*, Wiley, 2000.

[AR08] Mark Ainsworth and Richard Rankin, *Fully computable bounds for the error in nonconforming finite element approximations of arbitrary order on triangular elements*, SIAM J. Numer. Anal. **46** (2008), no. 6, 3207–3232.

[BCD04] S. Bartels, C. Carstensen, and G. Dolzmann, *Inhomogeneous Dirichlet conditions in a priori and a posteriori finite element error analysis*, Numer. Math. **99** (2004), no. 1, 1–24.

[BCJ02] S. Bartels, C. Carstensen, and S. Jansche, *A posteriori error estimates for nonconforming finite element methods*, Numer. Math. **92** (2002), 233–256.

[Beb03] M. Bebendorf, *A note on the Poincaré inequality for convex domains*, Z. Anal. Anwendungen **22** (2003), no. 4, 751–756.

[Bra07] Dietrich Braess, *Finite elements - theory, fast solvers, and applications in solid mechanics*, Cambridge University Press, New York, 2007.

[Bra09] Dietrich Braess, *An a posteriori error estimate and a comparison theorem for the nonconforming P_1 element*, Calcolo **46** (2009), no. 2, 149–155.

[BS08] S.C. Brenner and L.R. Scott, *The mathematical theory of finite element methods*, third ed., Texts in Applied Mathematics, Springer-Verlag, 2008.

[Car05] C. Carstensen, *A unifying theory of a posteriori finite element error control*, Numer. Math. **100** (2005), no. 4, 617–637.

[CDN10] S. Cochez-Dhondt and S. Nicaise, *A posteriori error estimators based on equilibrated fluxes*, Comput. Methods Appl. Math. **10** (2010), no. 1, 49–68.

[CF99] C. Carstensen and S.A. Funken, *Fully reliable localised error control in the fem*, SIAM J. Sci. Comput. **21** (1999), no. 4, 1465–1484 (electronic).

[CM10] C. Carstensen and Christian Merdon, *Estimator competition for Poisson problems*, J. Comput. Math. **28 (3)** (2010), 309–330.

[CMx3] Carsten Carstensen and Christian Merdon, *Effective postprocessing for equilibration a posteriori error estimators (accepted)*.

[DDPV96] E. Dari, R. Duran, C. Padra, and V. Vampa, *A posteriori error estimators for nonconforming finite element methods*, RAIRO Modél. Math. Anal. Numér. **30** (1996), no. 4, 385–400.

[DM98] Philippe Destuynder and Brigitte Métivet, *Explicit error bounds for a nonconforming finite element method*, SIAM J. Numer. Anal. **35** (1998), no. 5, 2099–2115 (electronic).

[GR86] V. Girault and P. A. Raviart, *Finite element methods for Navier Stokes equations*, Springer-Verlag, 1986.

[Han05] Weimin Han, *A posteriori error analysis via duality theory*, Advances in Mechanics and Mathematics, vol. 8, Springer-Verlag, New York, 2005, With applications in modeling and numerical approximations.

[HHW96] Ronald H.W. Hoppe and Barbara Wohlmuth, *Element-oriented and edge-oriented local error estimators for nonconforming finite element methods*, 1996.

[HW96] Ronald H. W. Hoppe and Barbara Wohlmuth, *Element-oriented and edge-oriented local error estimators for nonconforming finite element methods*, RAIRO Modél. Math. Anal. Numér. **30** (1996), no. 2, 237–263.

[Joh98] Volker John, *A posteriori L2-error estimates for the nonconforming P1/P0-finite element discretization of the Stokes equations*, J. Comput. Appl. Math. **96** (1998), no. 2, 99–116.

[Kim07] Kwang Y. Kim, *A posteriori error analysis for locally conservative mixed methods*, Math. Comp. **76** (2007), no. 257, 43–66 (electronic). MR 2261011 (2008b:65134)

[LW04] R. Luce and B. I. Wohlmuth, *A local a posteriori error estimator based on equilibrated fluxes*, SIAM J. Numer. Anal. **42** (2004), no. 4, 1394–1414.

[MZS10] Shipeng Mao, Xuying Zhao, and Zhongci Shi, *Convergence of a standard adaptive nonconforming finite element method with optimal complexity*, Appl. Numer. Math. **60** (2010), no. 7, 673–688.

[PW60]   L. E. Payne and H. F. Weinberger, *An optimal Poincaré inequality for convex domains*, Arch.
          Rat. Mech. Anal. **5** (1960), 286–292.

[Rab10]   H. Rabus, *A natural adaptive nonconforming fem of quasi-optimal complexity*, CMAM **10** (2010),
          no. 3, 316–326.

[Rep08]   Sergey Repin, *A posteriori estimates for partial differential equations*, Radon Series on Computa-
          tional and Applied Mathematics, vol. 4, Walter de Gruyter GmbH & Co. KG, Berlin, 2008.

[Val09]   Jan Valdman, *Minimization of functional majorant in a posteriori error analysis based on H(div)
          multigrid-preconditioned cg method*, Advances in Numerical Analysis **2009** (2009).

[Ver96]   Rüdiger Verfürth, *A review of a posteriori error estimation and adaptive mesh-refinement tech-
          niques*, Wiley-Teubner series in advances in numerical mathematics, Wiley-Teubner, 1996.

[VHS11]   M. Vohralík, A. Hannukainen, and R. Stenberg, *A unified framework for aposteriori error es-
          timation for the stokes problem*, Accepted for Numer. Math. (2011), HAL Preprint 00470131,
          http://hal.archives–ouvertes.fr/hal–00470131/en/.

[Voh07]   Martin Vohralík, *A posteriori error estimates for lowest-order mixed finite element discretizations
          of convection-diffusion-reaction equations*, SIAM J. Numer. Anal. **45** (2007), no. 4, 1570–1599
          (electronic).

[Voh11]   ⸺, *Guaranteed and fully robust a posteriori error estimates for conforming discretizations of
          diffusion problems with discontinuous coefficients*, J. Sci. Comput. **46** (2011), no. 3, 397–438.

Humboldt-Universität zu Berlin, Unter den Linden 6, 10099 Berlin, Germany;
Department of Computational Science and Engineering, Yonsei University, 120-749 Seoul,
Korea.

  E-mail address: cc@mathematik.hu-berlin.de and merdon@mathematik.hu-berlin.de